

# Random advection-diffusion models and their statistics

Stefano Lepri,<sup>1,2</sup> Paolo Politi,<sup>1,2</sup> and Arkady Pikovsky<sup>3</sup>

<sup>1</sup>*Consiglio Nazionale delle Ricerche, Istituto dei Sistemi Complessi,  
Via Madonna del Piano 10 I-50019 Sesto Fiorentino, Italy.*

<sup>2</sup>*Istituto Nazionale di Fisica Nucleare, Sezione di Firenze,  
via G. Sansone 1, I-50019 Sesto Fiorentino, Italy*

<sup>3</sup>*Department of Physics and Astronomy, University of Potsdam  
Karl-Liebknecht-Str 24/25, Bldg 28 D-14476, Potsdam, Germany*

We study the statistics of a one-dimensional randomly advected field with diffusion. The motivation for this setup comes from a straightforward interpretation as advection of particles in one-dimensional turbulence, but it is also related to a problem of synchronization of dynamical systems driven by common noise. A general class of lattice models describing the joint effect of random advection and diffusion for an ensemble of particles is introduced. It consists of a general microscopic random update rule and encompasses as specific cases, some models studied in the literature, like the Kang-Redner, Kipnis-Marchioro-Presutti, Takatsu-Taguchi etc. For finite lattices, we study both the coagulation of an initially spread field (interpreted as roughening), and the statistical steady-state properties. We distinguish two main size-dependent regimes, depending on the strength of the advection term and on the lattice size. Using numerical simulations and mean-field approach, we study the statistics of the field. For weak diffusion, we unveil a characteristic hierarchical structure of the field. We also connect the model and the iterated function systems concept.

## I. INTRODUCTION

Advection and diffusion are two basic transport phenomena occurring in diverse physical contexts. The former amounts to the motion of, for instance, small tracer particles (like a pollutant) transported by the movement of a surrounding fluid. On the other hand, diffusion is caused by the familiar mechanism of Brownian random walk that causes a stochastic spreading of tracer particles due to the interaction with a solvent.

A particularly interesting case is where advection is a random process. In the applications to turbulence, there is a vast literature on the matter [1]. A celebrated example is the Kraichnan model for the advection of a passive scalar by a random flow [2]. In this case, one usually assumes an incompressible (solenoidal) velocity field [2] or a weakly compressible fluid [3]. As it is known, the former case is related to Hamiltonian dynamical systems theory, as exemplified by Lagrangian chaos [4]. On the other hand, the issue of compressible fluids is less studied and corresponds to dissipative phase-space flows.

Besides the problem of passive scalar transport in fluids, the concept of advection is more general and applies in more abstract sense to spreading of an ensemble of trajectories in phase space of a dynamical system subject to a common regular or irregular phase velocity field. Examples of this setup appear in neurosciences and other fields. Another interesting application concerns transport in active media [5] as it occurs for light in disordered and amplifying systems [5, 6].

Mathematically, a description of the problem in the continuum limit requires dealing with a stochastic partial differential equation, that are notoriously hard to deal with. From a more statistical-mechanics point of view, it is thus helpful to consider simple *discrete* microscopic or mesoscopic models of the dynamics that respect

some fundamental features of the problem. Such an approach is insightful as it allows to simulate the process straightforwardly. In this work, we follow this strategy to take a fresh look at the problem where random advection and diffusion are *both* present. We introduce a general class of stochastic lattice models where microscopic moves mimic the two basic mechanisms, namely the collective random motion of particles induced by the common advecting field and the spreading caused by microscopic diffusion (this distinction will be made clear in the following). For simplicity, we deal with a one-dimensional lattice but the dynamics is easily generalized to higher dimensions or graphs. We anticipate the class to encompass various models considered previously in the literature as particular cases.

The primary model we are going to study depends on a single parameter  $\epsilon$  confined to the unitary interval  $[0, 1]$  and allowing for tuning the relative importance of advection and diffusion. We are interested both in the time dependence of the field evolving from an initial uniform state and in the properties of the statistically stationary state that emerges at large times. In the former case, the typical phenomena are coarsening and roughening, namely how clusters merge and how the field variance grows in time. Also, the steady-state statistics of the field is of great interest. We will report cases where the statistics is strongly non-Gaussian and we will be able to give a scaling description of the asymptotic state for any  $\epsilon$  and any size  $L$  of the system.

The paper is organized as follows. In Section II we describe the basic phenomenology of advection and diffusion in a smooth, random field and introduce the basic distinction between macroscopic (collective) and microscopic diffusion. The general class of models with stochastic microscopic dynamics is defined in Section III. Particular cases corresponding to various systems stud-

ied in the literature are examined there. Our analysis starts by considering the case of no microscopic diffusion for a finite lattice (Section IV) and its roughening properties. We then focus on various steady-state properties in Sections V, VI and VII. Conclusions are given in Section VIII, along with a brief comparison of our results with those given in the literature for other models with similar conservation laws. Some more technical aspects are relegated to the Appendix.

## II. PHENOMENOLOGY OF RANDOM ONE-DIMENSIONAL ADVECTION AND DIFFUSION

Let us start by discussing general qualitative concepts about one-dimensional random passive scalar advection. The starting point is an ensemble of “particles” with coordinates  $x_i(t)$  in a velocity field  $v(x, t)$ , so that the dynamics is simple

$$\frac{dx_i}{dt} = v(x_i, t). \quad (1)$$

We assume that the velocity field  $v(x, t)$  is a random function of time so that each particle displays a random one-dimensional motion. In order for the differential equation (1) to be well-posed, the field  $v(x, t)$  should be smooth enough in  $x$  (at least Lipschitz continuous). As a physical realization for the setup (1), let us consider two-dimensional convection in a vertically placed Hele-Shaw cell heated from below, with an open upper surface. For a large enough Rayleigh number, convection will be irregular (turbulent). Consider now particles floating on the surface; then they will be governed by Eq. (1), where  $v(x, t)$  is the velocity field on the surface of the cell.

The main macroscopic effect is the coagulation/clustering of particles. Indeed, if the coordinates of two particles coincide at  $t = 0$ :  $x_i(0) = x_j(0)$ , then their trajectories are identical at any later time, i.e.,  $x_i(t) \equiv x_j(t) = X(t) \forall t > 0$ , with  $\dot{X} = v(X, t)$  and  $X(0) = x_{i,j}(0)$ . A cluster of particles with identical positions is, therefore, a solution of Eq. (1). A second and equally important remark is that such a solution is stable in the sense that neighboring particles get effectively “attracted” to each other to form a cluster. To see this, suppose that the field  $v(x, t)$  is a smooth enough function of  $x$ , so that one can linearize (1) around a reference trajectory of a cluster  $X(t)$ , to obtain for a small perturbation  $\Delta x$

$$\frac{d}{dt} \Delta x = \Delta x \frac{\partial}{\partial x} v(X(t), t). \quad (2)$$

This linear equation with a random function of time  $v(X(t), t)$  defines the Lyapunov exponent

$$\lambda = \left\langle \frac{\partial}{\partial x} v(X(t), t) \right\rangle_t \quad (3)$$

so that asymptotically in time,  $\Delta x(t) \propto \exp[\lambda t]$ .

The main observation is that in one-dimensional continuous dynamics, the Lyapunov exponent cannot be positive, because the phase volume for a statistically stationary regime cannot grow indefinitely. Furthermore, it is unprobable for random fields that the Lyapunov exponent vanishes. Indeed, in non-random one-dimensional dynamics, the Lyapunov exponent can be either negative (a sink) or zero (e.g., a steady periodic motion over a periodic space profile). A randomness “mixes” these two situations, thus leading to a negative Lyapunov exponent. For a negative Lyapunov exponent,  $\Delta x \rightarrow 0$  as  $t \rightarrow \infty$ . This means that neighboring particles glue together (coagulate) and in a finite system, a stable cluster forms at long enough times. Since there *all* the particles have the same trajectory, we will refer to it as the *maximal cluster*. Also, since the cluster will perform a random motion, we will, for definiteness, refer to the such process as *macrodiffusion*.

We note here that coagulation to a maximal cluster also occurs in more general situations, provided the maximal Lyapunov exponent is negative. For example, such a situation is possible for two-dimensional advection as well, although in this case, there are two Lyapunov exponents, so the maximal one may become positive, and the cluster will be destroyed. One class of problems where a maximal cluster appears is irreversible aggregation, where a large number of small particles coalesce over time with no possibility of breaking up, see Ref. [7] and the literature therein. On the other hand, in the context of noise-driven dynamical systems, the effect of the formation of the maximal cluster has been termed *synchronization by common noise* and was first described in Refs. [8, 9], where an ensemble of identical systems (i.e., an ensemble of different initial conditions) driven by the same realization of noise was analyzed. In mathematical literature, equations of type (1) are called random dynamical systems and a maximal cluster state as described above represents a point random attractor in such a system [10]. The effect of synchronization by common noise also appears in neuroscience (there it is called reliability [11]), and in other fields [12, 13]. If the maximal Lyapunov exponent becomes positive (what is possible starting from dimension two), a point attractor undergoes a transition to a fractal one [14, 15]. In the context of passive scalar advection theory, such a transition, happening as compressibility of the underlying flow increases, was discussed in [16].

The nature of the macrodiffusion (i.e., whether it is normal or anomalous) depends on the actual statistical properties of the field  $v(x, t)$  (cf. [17]). In the examples considered below, we will limit to the case where spatial and temporal correlations of the velocity field decay rapidly, so that the macrodiffusion will be normal.

We stress that the arguments about attracting clustered states are valid for a large but finite system. This will be the case we consider in this paper, where we also will explore scaling relations as the size of the system

goes to infinity.

Although a clustered state is an attractor in the random advection dynamics (1), there can be several such attractors in degenerate situations. Indeed, if, e.g., the velocity field is odd in space  $v(-x, t) = -v(x, t)$ , then  $v(0, t) = 0$  and the particles starting in positive  $x > 0$  and negative  $x < 0$  domains never meet and never coagulate, so there are at least two attractors here. Below, we assume that such a degenerate situation does not occur, and we have one ergodic component: all the initially distributed particles evolve under (1) to one single maximal cluster.

The above concept of macrodiffusion should be juxtaposed with a familiar Brownian motion, as given by the Langevin equations

$$\frac{dx_i}{dt} = \sigma \xi_i(t), \quad (4)$$

where the microscopic noises  $\xi_i(t)$  are zero-average, independent (i.e., different for different particles) Gaussian and white noises with  $\langle \xi(t) \rangle = 0$ ,  $\langle \xi_i(t) \xi_j(t') \rangle = 2\delta_{ij} \delta(t - t')$ . This noise leads to a diffusive spreading  $\sim \sigma^2 t$  of particles in the ensemble. We call this effect *microdiffusion* for a clear distinction with the above.

Our main goal in this paper is to contribute to an understanding of the behavior of an ensemble of particles, where both macro- and microdiffusion in a given random velocity field are present; namely, we combine (1) and (4) into an equation

$$\frac{dx_i}{dt} = v(x_i, t) + \sigma \xi_i(t). \quad (5)$$

We illustrate different regimes in the dynamics of (5) in Fig. 1.

Equation (5) can be considered as a Langevin equation so that the evolution of the probability density  $w(x, t)$  of an ensemble of particles obeys the Fokker-Planck equation

$$\frac{\partial}{\partial t} w + \frac{\partial}{\partial x} (v(x, t)w) = \sigma^2 \frac{\partial^2 w}{\partial x^2}. \quad (6)$$

We stress that this equation includes averaging over the microscopic noise terms  $\xi(t)$  but still contains the random function  $v(x, t)$ , which is common for all the particles. Thus, formally this equation is a stochastic partial differential equation.

Our main interest is in the statistical properties of the density  $w(x, t)$ . As argued above, in the absence of microdiffusion,  $\sigma = 0$ , the asymptotic state is a point attractor (cluster) which moves randomly:  $w(x, t) = \delta(x - X(t))$ . This singular solution becomes “smeared” by a finite microdiffusion  $\sigma > 0$ . However, the details of this continuous random field  $w(x, t)$  are not clear a priori, and the goal of this paper is to contribute to understanding the statistical properties of the distribution density  $w$ .

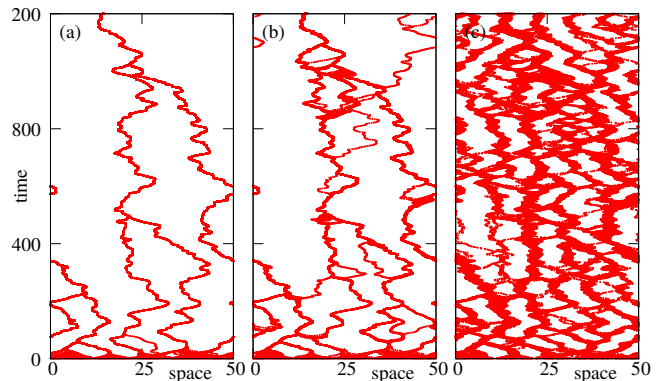


FIG. 1. Dynamics of a set of 200 particles, initially uniformly distributed, according to Eq. (5) for different levels of microdiffusion  $\sigma$ , for the same realization of random field  $v(x, t)$  (this field is taken as a chaotic solution of the Kuramoto-Sivashinsky equation, cf. [17]). Panel (a): microdiffusion-free case  $\sigma = 0$ , here one observes a perfect formation of the maximal cluster. Panel (b): small noise  $\sigma = 0.005$ , here some particles due to noise split from the largest cluster, which, however, contains most of them. Panel (c): large noise  $\sigma = 0.3$ , here the distribution of particles is inhomogeneous, but there are no dominating clusters.

### III. LATTICE MODELS

It is computationally rather costly to simulate Eq. (6) on a large domain and for small  $\sigma$ . A convenient approach to finding scaling properties of random advection is to explore proper lattice models. In a lattice model, the field is discrete in space, and therefore one cannot perform a continuous stability analysis of a cluster state like in Eq. (2) above. Indeed, if one takes the continuous in space model (1), then a natural assumption is that the velocity fields at large distances are independent, but at small distances (at which the linearization (2) is valid) it is smooth. Thus, if one takes two particles at a large initial distance, they first diffuse independently, and only when they are close enough to each other do they merge according to the Lyapunov exponent (3). A lattice model can imitate the first stage of independent diffusion but replaces the second stage of exponential convergence with an abrupt coalescence. Furthermore, the lattice models below are formulated in a discrete time. In these models one defines a conserved “mass field”  $u_k(t)$ , where  $k$  is the lattice site, and  $t$  is discrete time. This field should be interpreted as a discretized density  $w(x, t)$  of advected particles from equation (6).

#### A. Generic two-site models

We start with a rather generic setup and then focus on two particular lattice models that will be considered below. We assume that the models for a continuous field on a lattice are formulated as follows:

1. A pair of neighboring sites,  $(k, k + 1)$ , is chosen randomly.
2. The fields at these sites,  $u_k, u_{k+1}$ , are redistributed according to a deterministic (parameters fixed) or stochastic (parameters chosen from a distribution) linear rule,

$$u'_k = (1 - a)u_k + bu_{k+1} \quad (7)$$

$$u'_{k+1} = au_k + (1 - b)u_{k+1}, \quad (8)$$

where the primes indicate the masses after a move and where we have implemented mass conservation.

Therefore, the rule is generically described by a stochastic matrix depending on two parameters  $0 \leq a, b \leq 1$ :

$$A(a, b) = \begin{pmatrix} 1 - a & b \\ a & 1 - b \end{pmatrix}.$$

If  $a \neq b$ , the distribution is asymmetric. Thus, for fixed  $a \neq b$ , one applies matrices  $A(a, b)$  and  $A(b, a)$  with probabilities  $1/2$ . Such a symmetrization might not be needed if  $a, b$  are chosen as random variables.

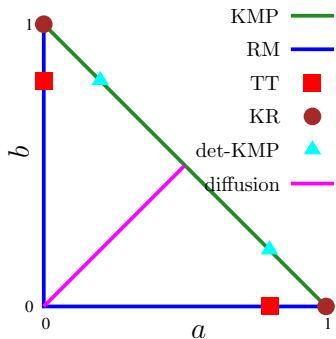


FIG. 2. Different models in terms of parameters  $(a, b)$ . Cases TT, KR, and det-KMP with fixed parameters (except for diffusion) are shown with markers (for definiteness, we take  $\epsilon = 0.8$ ); cases KMP and RM, where parameters are random, are shown with lines on which the values of these parameters lie.

In terms of these parameters, different models from the literature can be described as follows:

- **Kang-Redner (KR) model** [18] (see a detailed description in section III B below) corresponds to  $a = 1, b = 0$ : all the mass of a random site  $i$  is transferred to a random neighbour  $i \pm 1$ .
- **Takayasu-Taguchi (TT) model** [19] (see a detailed description in section III C below) corresponds to  $a = 1 - \epsilon, b = 0$ : the fraction  $a$  of the mass of a random site  $i$  is transferred to a random neighbour  $i \pm 1$ .
- **Kipnis-Marchoro-Presutti (KMP) model** [20] (see discussion in section VIII) corresponds to  $a = 1 - b = \xi$ , where  $\xi$  is uniformly distributed  $0 \leq \xi \leq 1$ : the total mass of a random pair of neighboring sites is randomly redistributed between them.

- **Rajesh-Majumdar (RM) model** [21] (see discussion in section VIII) in the limiting case of a sequential update is a random version of TT model  $a = \xi, b = 0$ , where  $\xi$  is uniformly distributed  $0 \leq \xi \leq 1$ .

- **Deterministic KMP (det-KMP) model** (it looks like this model has not been considered before) corresponds to  $a = \epsilon, b = 1 - \epsilon$ : a certain portion of the total mass of a random pair of neighboring sites is distributed between them in a fixed proportion.

- **Diffusion** This is a situation when  $a = b$  (either fixed or random): a random site gains (or loses) a fraction of the mass difference between it and a neighboring site.

In this paper, we focus on the KR and TT lattice models and discuss the relation to KPM, RM, det-KPM, and some models based on the particle dynamics in section VIII.

## B. Kang-Redner model

This setup is attributed to Smoluchowski; it describes coagulation without microdiffusion (i.e., at  $\sigma = 0$ ). We outline it following the paper [18] (where this model is also discussed in dimensions higher than one). In this Kang-Redner (KR) model, the field  $u_k$  is fully discrete: on each site of a discrete, regular one-dimensional lattice, the mass is an integer number of “particles”,  $u_k = 0, 1, 2, \dots$ . Such masses macrodiffuse with a constant diffusion constant, according to the following sequential update: at each time step, a site  $k$  is chosen at random, along with the direction of motion ( $\pm$ , also chosen at random). Then the mass migrates from site  $k$  to the neighboring site:

$$\begin{aligned} u_k(t+1) &= 0, \\ u_{k\pm 1}(t+1) &= u_{k\pm 1}(t) + u_k(t). \end{aligned} \quad (9)$$

This model is sometimes called the  $A_i + A_j \rightarrow A_{i+j}$  kinetic reaction [7]. Clearly, on a finite lattice of size  $L$ , the distribution of masses converges to a state where all the particles occupy the same lattice site, and this maximal cluster performs a random walk.

The relaxation dynamics towards such a final state is characterized by the temporal evolution of the probability  $c_m(t)$  to have a cluster of  $m > 0$  particles. In one dimension and in the infinite domain, the authors of [18] provide the following scaling relation for  $c_m(t)$ :

$$\begin{aligned} c_m(t) &\sim \frac{m}{t^{3/2}} f\left(\frac{m}{t^{1/2}}\right), \quad m > 0, \\ \text{where } f(x) &\rightarrow \begin{cases} 1 & x \ll 1, \\ 0 & \text{(rapidly)} \quad x \gg 1. \end{cases} \end{aligned} \quad (10)$$

A similar result,  $c_m(t) \sim \frac{m}{t^{3/2}}$  valid for  $m \ll t^{1/2}$  is derived in [22]. We notice here that one can also formulate the KR model for masses that are not integers, but any non-negative real numbers (as is, e.g., assumed in the Takayasu-Taguchi model below). The phenomenology is the same: in the course of time, masses coagulate, and in a finite system, eventually, one moving maximal cluster contains all the initial mass. However, in this case, one has to generalize the discrete distribution  $c_m(t)$  into a continuous one; thus, we stick to the original Kang-Redner formulation for discrete particles.

### C. Takayasu-Taguchi model

In this work, we will focus on another microscopic model, first introduced by Takayasu and Taguchi (TT) in Ref. [19]. It is defined for a continuous lattice field  $u_k(t)$ , defined on sites  $k = 1, \dots, L$  (with periodic boundary conditions) and discrete time,  $t = 0, 1, 2, \dots$ . The dynamical rule is very similar to that in the KR model. For a randomly chosen site  $k$  and a randomly chosen “direction”  $\pm$ , the field is updated as

$$\begin{aligned} u_k(t+1) &= \epsilon u_k(t), \\ u_{k\pm 1}(t+1) &= u_{k\pm 1}(t) + (1 - \epsilon)u_k(t). \end{aligned} \quad (11)$$

The parameter  $0 \leq \epsilon < 1$  gauges the strength of field transport, because a fraction  $(1 - \epsilon)$  of the mass  $u_k$  is transported to a neighboring site and added to  $u_{k\pm 1}$  [23] (the case  $\epsilon = 1$  is trivial because there is no dynamics). By construction, the dynamics conserves the total mass,  $\sum_k u_k$ .

The TT dynamics entails both macro- and microdiffusion, their relative strengths being controlled by the parameter  $\epsilon$ . This follows from the two interesting limits.

1. For  $\epsilon \rightarrow 1$  the advection is weak, so the microdiffusion is relatively strong. In this case, at each step, a small portion of the field at a randomly chosen site is transferred left or right [24].
2. On the other hand, the case  $\epsilon = 0$  is one without microdiffusion but with pure random advection. It is also termed irreversible aggregation in Ref. [19]. Here, the fields at neighboring sites merge (coagulate), but no further splitting is possible. In fact, one can easily see that for  $\epsilon = 0$  the TT model (11) is essentially the same as the KR model (9), the only difference being the allowed set of values of  $u_k$ : in the KR model these values are integers, while in the TT model, they are non-negative real numbers. However, this difference appears to be irrelevant for large systems and for large times when clusters with large occupations emerge.

It is also to be mentioned that some variants of the TT model, including external injection, have been considered in Refs. [25, 26].

### D. Takayasu-Taguchi model with global coupling

In the following, we will also consider a variant of the TT model with *global* interaction. By this we mean that the exchange does not occur between the neighbors but rather between two independently randomly chosen sites  $k, m$ . Evolution follows the same rule,

$$\begin{aligned} u_k(t+1) &= \epsilon u_k(t), \\ u_m(t+1) &= u_m(t) + (1 - \epsilon)u_k(t). \end{aligned} \quad (12)$$

### E. The TT model as an Iterated Function System

The TT model has a remarkable mathematical interpretation as an Iterated Function System (IFS) with probabilities [27]. Indeed, each advection event in (11) is a linear contracting transformation of the vector  $\{u_k\}$ , and there are altogether  $2L$  different such transformation ( $L$  sites multiplied by two possible transport directions). Thus the probability for one particular transformation is  $(2L)^{-1}$ . Evolution is a composition of these transformations and fulfills the definition of an Iterated Function System (Chapter IX of book [27]). Typically, IFSs are used to produce fractal measures. We show in Appendix A that, indeed, one gets a fractal distribution (although not for all values of  $\epsilon$ ) in small lattices with  $L = 2, 3$ . In this paper, we are mainly interested in the case of large systems  $L \gg 1$ ; thus, we will focus not on the fractal properties of the field  $\{u_k\}$  (which are anyhow hardly accessible in numerics), but on the statistical properties.

## IV. STATISTICAL PROPERTIES OF THE KR MODEL ON A FINITE LATTICE

In this section, we report on the scaling properties of the coagulation process on finite lattices without microdiffusion. This corresponds to the KR model (9) or to the TT model (11) with  $\epsilon = 0$ . In fact, this section aims to extend the scaling relation (10) (valid for an infinite system) to the case of lattices of finite size  $L$ .

In numerical simulations, we start with a uniform initial state  $u_k(0) = 1$ ,  $k = 1, \dots, L$ . Because in this section masses  $u_k(t)$  are integers, we refer to these quantities as “number of particles” at site  $k$ , or a “cluster of size  $u_k$ ”. As expected from the general discussion in Sec. II, the final state after all the particles coagulated to a single site (i.e., they form the maximal cluster of size  $L$ ) is  $u_k(t) = L\delta_{kj}$ , where  $j(t)$  is the random position of the maximal cluster. The characteristic diffusion time of a particle in the lattice of length  $L$  is  $T_d(L) = L^2$ . [Because in the models (9) and (11) the update is sequential, the time here and below is measured in units of  $L$  to give a possibility for every site to move in one effective time unit.] We thus expect that  $T_d(L)$  is the time required for the formation of the maximal cluster. We now discuss the dynamics in the two relevant regimes.

### A. Short times: $t \ll T_d$

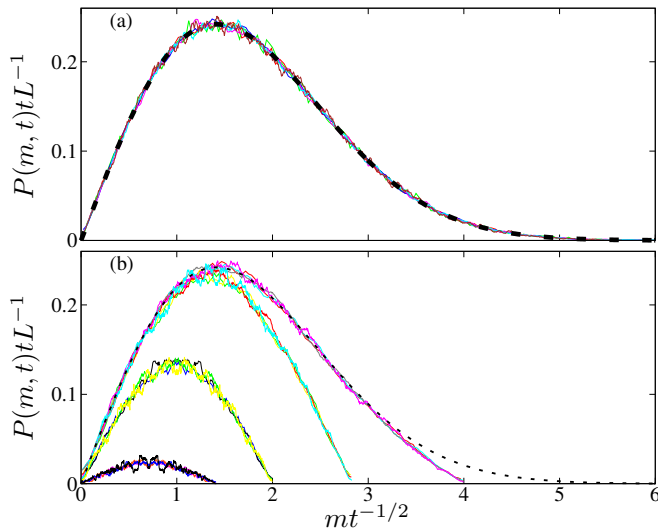


FIG. 3. Scaled probability distributions for the KR model at different times and lattice sizes. Panel (a): short times,  $t \ll T_d$ . Data for different  $L$  and different times (there are six nearly overlapping curves for  $L = 256, t = 512$ ;  $L = 256, t = 1024$ ;  $L = 512, t = 2048$ ;  $L = 512, t = 4096$ ;  $L = 1024, t = 16384$ ;  $L = 1024, t = 32768$ ) nearly perfectly overlap. The “guess” (14)  $\mathcal{F}(m/t^{1/2})$  (black dashed line) seems also to be very good. In all runs, averaging over 32768 realizations is performed. Additionally, the curves for  $L = 512$  and  $L = 1024$  are locally smoothed by a running window (otherwise, fluctuations are relatively large). Panel (b): the same but for large times. For four lattice lengths  $L = 128, 256, 512, 1024$  the instants of time correspond to  $t = T_d/16, T_d/8, T_d/4, T_d/2$  (nearly overlapping curves from top to bottom); with  $T_d = L^2$ . The curve  $\mathcal{F}(x)$  is also shown as the dashed line for comparison on this panel.

On this time scale, the scaling properties of the infinitely large system should hold. Indeed, KR give a scaling relation (10) (on an infinite lattice) for the average (over realizations of random advection) number of sites  $P(m, t)$  possessing a cluster of mass  $m > 0$  at time  $t$ . We expect this relation to hold on a finite lattice for small times. To compare results for different lattice sizes  $L$ , it is convenient to modify the scaling of (10) by multiplying by  $L$  (to pass from a probability to an average number of sites) and incorporating a factor  $m/t^{1/2}$  in the scaling function, so that

$$P(m, t) = t^{-1} L F_1(mt^{-1/2}). \quad (13)$$

Because  $L = \sum_m m P(m, t) \approx \int_0^\infty dm m P(m, t)$ , we conclude that normalization of  $F_1(x)$  is independent of  $L$ :

$$\int_0^\infty dx x F_1(x) = 1.$$

It is noteworthy that  $\sum_m P(m, t)$  (the total number of non-empty sites) is not normalized to  $L$ . In fact,

$\sum_m P(m, t) \simeq L/\sqrt{t}$ , which is the equivalent of the relation  $\sum_m c_m(t) \simeq t^{-1/2}$  given by Kang and Redner [18].

In Fig. 3(a), we show the simulations for  $L = 256, 512, 1024$ . We observe that (i) The data for different  $L$  and  $t$  nearly perfectly collapse, and (ii) A guess (black dashed line) in form of a simple analytical expression

$$\mathcal{F}(x) = \frac{x}{\sqrt{4\pi}} \exp\left[-\left(\frac{x}{2}\right)^2\right] \quad (14)$$

provides a very close fit of the observed data.

### B. Large times: $t \lesssim T_d$

For large times  $t \approx T_d$ , when the probability for the maximal cluster to exist  $P(L, t)$  is not negligible, the distribution  $P(0 < m < L, t)$  deviates from the one for infinite lattices, as shown in Fig. 3(b). Nevertheless, the distributions overlap for the same values of  $t/T_d$ . This observation suggests a finite-size generalization of scaling (13) of the form

$$P(m, t) = t^{-1} L F_2(mt^{-1/2}, m/L) + \delta_{m,L} P(L, t), \quad (15)$$

where in  $F_2$ , one has  $m < L$  (in other words, this function describes all clusters which are less than the maximal one) and  $\delta_{ij}$  is the Kronecker delta. The separation into two parts, the maximal cluster and the rest allows for using a continuous approximation for  $F_2$ . This scaling function now depends on two arguments,  $F_2(x, y)$ ,  $x = m/t^{1/2}$ ,  $y = m/L$  and must satisfy the following properties: (i) As  $L \rightarrow \infty$ , the scaling (13) must hold, thus  $F_2(x, 0) = F_1(x)$ ; (ii) There is no cluster with a size larger than  $L$  (and the maximal cluster of size  $L$  is not included to the distribution), thus  $F_2(x, y \geq 1) = 0$  [28]. From the normalization  $L = \sum_m m P(m, t)$  it directly follows the expected scaling for the probability of the maximal cluster:

$$P(L, t) = 1 - L^{-1} \int_0^\infty dm m t^{-1} L F_2\left(\frac{m}{t^{1/2}}, \frac{m}{L}\right) = s(t/L^2). \quad (16)$$

This relation is verified in Fig. 4.

We check the validity of Eq. (15) in Fig. 5. Here, we plot the distributions, rescaled according to Eq. (15), for several different fixed values of  $x = m/t^{1/2}$ , namely we plot  $G(m, t) = tL^{-1}P(m, t)/\mathcal{F}(mt^{-1/2})$  versus  $y = m/L$ . For each  $x$  considered, one can see a nice overlap of data obtained for several different sizes  $L = 128, 256, 512$ , supporting the Ansatz (15). As expected,  $G$  tends to 1 for  $x \rightarrow 0$  and vanishes for  $x \rightarrow 1$ . Another confirmation of scaling (15) is the bottom panel of Fig. 3.

### C. Roughening properties in KR model

Let us now describe the mass distribution  $u_k(t)$  interpreting it as an “interface” profile, whose width  $W(L, t, \epsilon)$

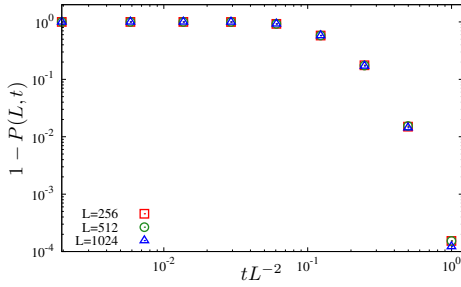


FIG. 4. Probability for the maximal cluster with occupation  $L$  to occur, Eq. (16), as a function of the scaled time  $t/L^2$ , for different  $L = 256, 512, 1024$ .

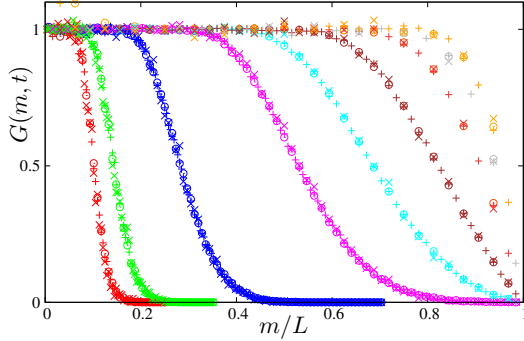


FIG. 5. Plot of the rescaled distributions  $G(m, t) = tL^{-1}P(m, t)/\mathcal{F}(mt^{-1/2})$  at different values of  $mt^{-1/2}$  [different colors: from top right to bottom left,  $mt^{-1/2} = 4$  (yellow),  $mt^{-1/2} = 3.46$  (grey),  $mt^{-1/2} = 2.83$  (dark red),  $mt^{-1/2} = 2$  (brown),  $mt^{-1/2} = 1.41$  (cyan),  $mt^{-1/2} = 1$  (magenta),  $mt^{-1/2} = 0.5$  (blue),  $mt^{-1/2} = 0.25$  (green),  $mt^{-1/2} = 0.177$  (red)] as a function of the rescaled variable  $y = m/L$ , for  $L = 128$  (open circles),  $L = 256$  (pluses), and  $L = 512$  (crosses).

is defined as usual in the following way:

$$W^2 = \langle (u - \langle u \rangle)^2 \rangle, \quad (17)$$

where  $\langle \cdot \rangle$  is both a spatial and a statistical average. Since this quantity will also be used later on, we made explicit the dependence on the parameter  $\epsilon$ , which distinguishes the TT model from the KR model (the models are equivalent for  $\epsilon = 0$ ).

Since the field is conserved, with our choice of the initial conditions  $\langle u \rangle = 1$  always. Following the Family-Vicsek scaling approach [29], we can write

$$W(L, t, 0) \sim L^\chi g\left(\frac{t}{L^z}\right), \quad (18)$$

where  $g(\xi)$  is a suitable scaling function with  $g(\xi) \sim \xi^\beta$  for  $\xi \ll 1$  and  $g(\xi) \sim 1$  for  $\xi \gg 1$ , so that  $W(L, t, 0) \sim t^\beta$  at short times ( $t \ll L^z$ , growth regime) and  $W(L, t, 0) \sim L^\chi$  at long times ( $t \gg L^z$ , saturated regime). The growth exponent  $\beta$ , the roughness exponent  $\chi$ , and the dynamical exponent  $z$  are related by  $\chi = \beta z$ .

In the specific case, we are considering in this Section (KR model), it is clear that the crossover time between the two regimes is given by the diffusive time  $T_d = L^2$ , so that  $z = 2$ . At short times we can make use of the scaling relation (13) for the probability to have a height  $k$ :

$$L^{-1}P(m, t) = \begin{cases} t^{-1}F_1(mt^{-1/2}) & m > 0, \\ 1 - \int_0^\infty t^{-1}F_1(mt^{-1/2}) dm = 1 - \frac{1}{\sqrt{\pi t}} & m = 0. \end{cases}$$

(in the last expression, we calculated the integral using function (14)). Thus the width can be computed explicitly using expression (14) for  $F_1$ :

$$W^2 = \int_0^\infty L^{-1}P(m, t)(m-1)^2 dm = \frac{4t^{1/2}}{\sqrt{\pi}} + 3.$$

Because the scaling holds for  $t \gg 1$ , we can assume

$$W \approx 2\pi^{-1/4} t^{1/4},$$

what yields the exponent  $\beta = 1/4$  and therefore  $\chi = 1/2$ . Altogether, we come to the scaling relation

$$W(L, t, 0) = L^{1/2} g\left(\frac{t}{L^2}\right). \quad (19)$$

This theoretical prediction is successfully checked in Fig. 6. The scaling function  $g(t/L^2)$  could be formally expressed in terms of the scaling function  $F_2(x, y)$ , but this would be a futile exercise, especially because we do not know the analytic form of  $F_2(x, y)$  (while we do have a very good expression for  $F_1(x)$ !).

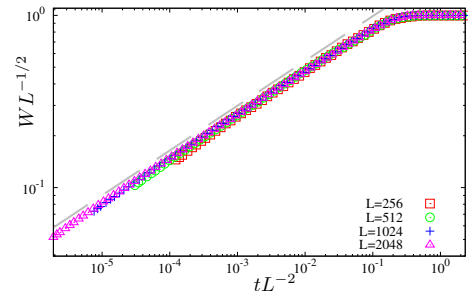


FIG. 6. Evolution of the width  $W(L, t, 0)$  in the KR model for different  $L$ , in the rescaled coordinates. The gray dashed line has slope 0.26, close to the exponent  $\beta$  predicted by Eq. (19). Data collapse on the scaling function  $g(t/L^2)$ .

At first glance, one may argue that  $\beta = 1/4$  and  $\chi = 1/2$  are the Edwards-Wilkinson (EW) roughening exponents in  $d = 1$ . However, this is just a coincidence because, at variance with EW, the distributions are *not* Gaussian. This should be traced back to the fact that, in the present model, the total mass is conserved, while in EW, it is not (see, however, a discussion of the conserved EW in Sec. VI B below).

In this respect, mass conservation might inspire one to compare the model under consideration with the conserved KPZ equation [30–32]. In one dimension, it reads

$$\begin{aligned} \frac{\partial \phi}{\partial t} &= -\nabla^2[\kappa \nabla^2 \phi + \lambda |\nabla \phi|^2] + \eta(x, t), \\ \langle \eta \rangle &= 0, \\ \langle \eta(x, t) \eta(x', t') \rangle &= -2D \nabla^2 \delta(x - x') \delta(t - t'), \end{aligned} \quad (20)$$

and fulfills mass conservation  $\int \phi(x, t) dx = \text{const.}$  However, the dynamic exponents characterizing roughening in this equation are  $z = 11/3$ ,  $\beta = 1/11$  and  $\chi = 1/3$  [30], which are distinctly different from ours. This is not surprising because there are two basic differences between (6) and (20): (i) In (20) the noise is additive and in (6) it is multiplicative; (ii) CKPZ equation is nonlinear while the random advection equation (6) is linear.

## V. EVOLUTION TO A STATIONARY STATE IN THE TT MODEL: OVERALL PICTURE

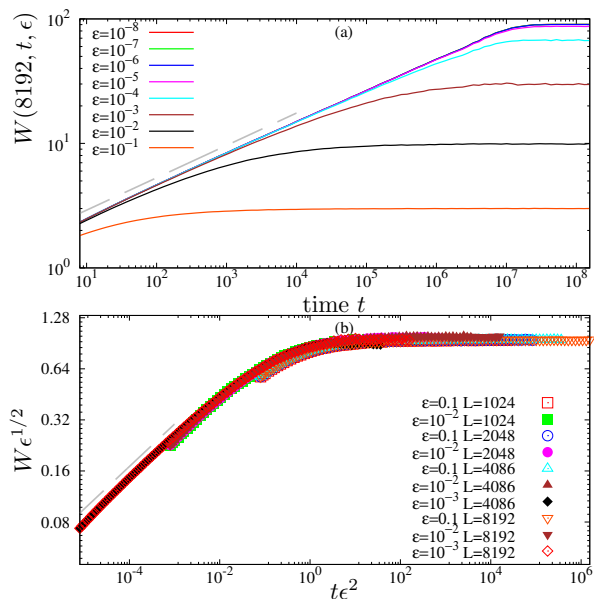


FIG. 7. Panel (a): field widths  $W(L, t, \epsilon)$  as a function of time, for different  $\epsilon$  and  $L = 8192$ . Panel (b): Widths of the field in dependence on time for different  $\epsilon, L$  in scaled coordinates. The dashed line has a slope of 0.26, which is close to the theoretical value 0.25 derived for  $\epsilon = 0$ .

Let us now turn to the case where parameter  $\epsilon$  in (11) is non-zero. In other words, both macrodiffusion and microdiffusion are present. We first performed the same roughening experiment as above but with the TT model. The results for different values of  $L$  and  $\epsilon$  are presented in Fig. 7. Both panels clearly indicate that, for a finite system, a statistically stationary regime establishes at long times. However, the evolution of the width crucially depends on parameter values  $\epsilon, L$ . In panel (a) of Fig. 7,

where we fix  $L = 8192$ , one can clearly see that the values of  $\epsilon$  can be separated into two ranges. For  $\epsilon \lesssim 10^{-5}$ , there is no significant  $\epsilon$ -dependence in  $W(L, t, \epsilon)$ ; the curves follow the roughening in the KR model (19). In contradistinction, for  $\epsilon \gtrsim 10^{-4}$ , the dependence of  $W(L, t, \epsilon)$  on  $\epsilon$  is significant, and the saturated width  $W(L, \infty, \epsilon)$  decreases with  $\epsilon$ . Therefore, for large values of  $\epsilon$ , we plot the data in another scaling that includes  $\epsilon$ , in Fig. 7(b). Now the data for different  $L$  overlap, which indicates that the “roughening” is not  $L$ -dependent. In other words, in this regime, there is no true roughening because the saturated width is system size-independent (but depends on the parameter  $\epsilon$ ).

A clean way to analyze the separate effects of the system size  $L$  and of the parameter  $\epsilon$  is to focus on the asymptotic, time-independent width  $W(L, \infty, \epsilon)$ . This is done in Fig. 8 where we plot  $W(L, \infty, \epsilon)/L^{1/2}$  versus  $\epsilon L/(1 - \epsilon)$ . The data of Fig. 8 cover a wide range of values of  $L$  and  $\epsilon$  and clearly indicate for the existence of two types of stationary states:

- **Macrodiffusion-dominated regime.** This regime corresponds to the leftmost part of the graph where the scaled width  $WL^{-1/2}$  does not depend on  $\epsilon$ . Here the width scales  $W \sim L^{1/2}$  like in the KR model at  $\epsilon = 0$ . Nevertheless, the state here is nontrivial and will be discussed in detail in Section VII below.
- **Microdiffusion-dominated regime.** This regime corresponds to the right-most part of the curves in Fig. 8, where the scaling  $WL^{-1/2} \sim \left(\frac{\epsilon}{1-\epsilon}L\right)^{-1/2}$  holds. This means that here the width does not depend on the system size  $L$ :  $W \sim \left(\frac{\epsilon}{1-\epsilon}\right)^{-1/2}$ . We discuss this regime in Section VI below.

The crossover between two regimes occurs at  $\left(\frac{\epsilon}{1-\epsilon}L\right) \approx 1$ , i.e. at  $\epsilon L \approx 1$ . We remark that the microdiffusion-dominated regime is attained when  $\epsilon \gg 1/L$  but also for  $\epsilon \rightarrow 1$  and rather small  $L$ . A final comment about simulations is in order here. While it is relatively easy to vary parameter  $\epsilon$  in a wide range, for the length  $L$ , we can hardly significantly increase the range beyond several thousand.

Below in Sections VI and VII, we will focus on the detailed analysis of stationary regimes for microdiffusion- and macrodiffusion-dominated regimes, respectively.

## VI. STRONG MICRODIFFUSION $\epsilon > L^{-1}$

The discussion above shows that the system length is irrelevant here.

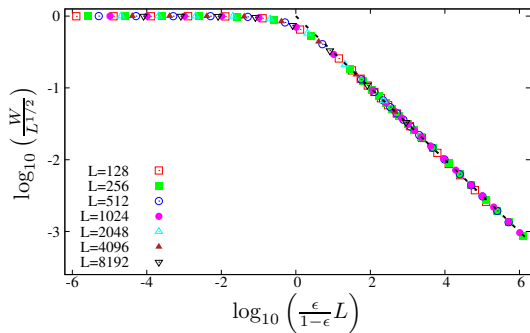


FIG. 8. Asymptotic ( $t \rightarrow \infty$ ) roughness  $W(L, \infty, \epsilon)$  as a function of the system size  $L$  and of the parameter  $\epsilon$ . Data collapse shows that  $W(L, \infty, \epsilon) = L^{1/2} f(L\epsilon/(1-\epsilon))$ , where the scaling function  $f(u)$  has the limiting behavior  $f(u) = 1$  for  $u \ll 1$  and  $f(u) = u^{-1/2}$  for  $u \gg 1$ . The dashed line has a slope of  $-1/2$ .

### A. Mean-field theory

We start with the mean-field theory, where spatial correlations are neglected (our approach is similar to that of Ref [19] but does not coincide with it). With probability  $1/2$ , each site either delivers part of its field to a neighbor, or receives a part of the neighbor's field. Thus, the updating rule for a field at a given site reads  $u \rightarrow \bar{u}$ ,

$$\bar{u} = \begin{cases} \epsilon u & \text{Prob } 1/2, \\ u + (1-\epsilon)v & \text{Prob } 1/2, \end{cases} \quad (21)$$

where  $v$  is the field of the neighbor. In the mean-field approach, we assume statistical independence of  $u$  and  $v$ , which have the same distribution. This allows for expressing the evolution of the density through a Perron-Frobenius operator

$$\begin{aligned} \bar{w}(x) &= \langle \delta(x - \bar{u}) \rangle = \frac{1}{2} \int_0^\infty du w(u) \delta(x - \epsilon u) + \\ &\frac{1}{2} \iint_0^\infty du dv w(u) w(v) \delta(x - u - (1-\epsilon)v) = \\ &= \frac{1}{2\epsilon} w\left(\frac{x}{\epsilon}\right) + \frac{1}{2} \int_0^{x(1-\epsilon)^{-1}} dv w(x - (1-\epsilon)v) w(v). \end{aligned} \quad (22)$$

Unfortunately, we cannot solve this equation analytically, except for the case  $\epsilon = 1/2$ , for which one can easily check that the solution is an exponential distribution  $w(u) = \exp(-u)$ . Indeed, in this case the calculation of the r.h.s. of (22) is straightforward:

$$\begin{aligned} w(2x) + \frac{1}{2} \int_0^{2x} dv e^{-x+v/2} e^{-v} &= \\ = e^{-2x} + \frac{e^{-x}}{2} \int_0^{2x} e^{-v/2} dv &= e^{-x}. \end{aligned}$$

It is however possible to express, for arbitrary  $\epsilon$ , all the moments  $M_n = \langle u^n \rangle$  explicitly in a recursive manner.

Indeed, directly from (21) it follows  $M_n = \frac{1}{2} \langle (\epsilon u)^n \rangle + \frac{1}{2} \langle (u + (1-\epsilon)v)^n \rangle$ , what begets

$$M_n = \frac{\sum_{k=1}^{n-1} \binom{n}{k} (1-\epsilon)^k M_{n-k} M_k}{1 - \epsilon^n - (1-\epsilon)^n}. \quad (23)$$

Since the total field is conserved, the value of  $M_1$  is arbitrary, and we may take  $M_1 = 1$ , as enforced in the numerical simulations. This yields  $\langle u^2 \rangle = 1/\epsilon$ , so that the mean width defined according to (17) is  $W^2 = M_2 - M_1^2 = \frac{1-\epsilon}{\epsilon}$ . Figure 8 proves that this result is correct in the large  $\epsilon L$  regime.

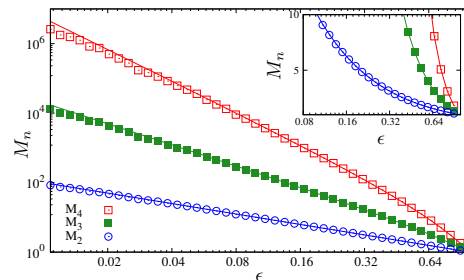


FIG. 9. Comparing numerically found moments 2-4 (markers, in a lattice of  $L = 1024$ ) with theoretical formulae (lines). The inset shows a region of large  $\epsilon$  with a linear scale of  $M_n$ -axis.

To test more thoroughly the accuracy of the approximations, in Fig. 9 we compare the mean-field values of the first three nontrivial moments with their numerical values. While the comparison looks like supporting the main assumption that the neighboring sites are statistically independent, an additional check for this dependence gives a different picture. For a quantitative characterization of the independence of two distributions  $w(u_n)$  and  $w(u_{n+d})$  at sites separated by distance  $d$  we use the mutual information

$$I(d) = \sum_{i,j} W_{ij} \log \frac{W_{ij}}{p_i q_j}.$$

where  $p_i$  and  $q_j$  are binned probabilities, and  $W_{ij}$  is the joint binned probability. For independent random variables, mutual information vanishes, but in real calculations, it is always positive. The values of  $I(d)$  for large distances  $d$  serve as “surrogates”, giving the numerical level of mutual information for practically independent distributions. The results (Fig. 10) suggest that the independence of neighbors might be *exact* for  $\epsilon \geq 0.5$ . But, instead, mutual dependence turns on for  $\epsilon < 0.5$ . On the other hand, even for  $\epsilon = 0.01$ , only some five neighboring sites are interdependent according to the mutual information criterion.

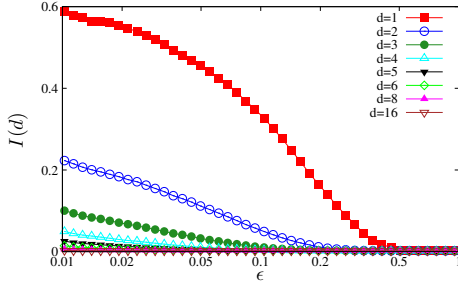


FIG. 10. Mutual information for different distances  $d$  between the sites. Details of calculations:  $L = 1024$ , number of patterns in statistical averaging 1024, number of bins 64 (bins are spaced so that all bins have the same probability  $1/64$ ).

### B. Limit of strong microdiffusion $\epsilon \rightarrow 1$

Let us rewrite the local TT model as an application of a matrix

$$A(\mu, \pm) = \begin{cases} \begin{pmatrix} 1 - \mu & 0 \\ \mu & 1 \end{pmatrix} & \text{prob } 1/2, \\ \begin{pmatrix} 1 & \mu \\ 0 & 1 - \mu \end{pmatrix} & \text{prob } 1/2. \end{cases}$$

where a portion  $\mu = 1 - \epsilon$  is moved to the right (to the left). To have a symmetric situation, suppose that this matrix is applied twice (thus, one has four combinations). Furthermore, we assume  $\mu \ll 1$ , in this case  $A(\mu, +)A(\mu, -) \approx A(\mu, -)A(\mu, +)$ . Then in the 1st order in  $\mu$

$$A^2 = \begin{cases} \begin{pmatrix} 1 - \mu & \mu \\ \mu & 1 - \mu \end{pmatrix} = I + \mu \begin{pmatrix} -1 & 1 \\ 1 & -1 \end{pmatrix} & \text{prob } 1/2, \\ \begin{pmatrix} 1 - 2\mu & 0 \\ 2\mu & 1 \end{pmatrix} = I + 2\mu \begin{pmatrix} -1 & 0 \\ 1 & 0 \end{pmatrix} & \text{prob } 1/4, \\ \begin{pmatrix} 1 & 2\mu \\ 0 & 1 - 2\mu \end{pmatrix} = I + 2\mu \begin{pmatrix} 0 & 1 \\ 0 & -1 \end{pmatrix} & \text{prob } 1/4. \end{cases}$$

(here,  $I$  is the unit matrix). To obtain a continuous in space formulation, we attribute operator  $\partial_{xx}$  to the first matrix, and operators  $\pm\partial_x$  to the second and the third matrices. In this way, we approximate the evolution with

$$\partial_t u(x, t) = \mu \partial_x (Vu) + \mu \partial_{xx} u, \quad V = \pm \frac{\Delta x}{\Delta t}.$$

Because  $V$  has independent values at different sites and different time steps, we can model velocity with a  $\delta$ -correlated noise field

$$\begin{aligned} \partial_t u(x, t) &= \mu \partial_x (\xi(x, t)u) + \mu \partial_{xx} u, \\ \langle \xi(x, t) \xi(x', t') \rangle &= \delta(x - x') \delta(t - t'). \end{aligned}$$

Rescaling time  $\mu t = \tau$  we obtain

$$\begin{aligned} \partial_\tau u(x, \tau) &= \mu^{1/2} \partial_x (\eta(x, \tau)u) + \partial_{xx} u, \\ \langle \eta(x, \tau) \eta(x', \tau') \rangle &= \delta(x - x') \delta(\tau - \tau'). \end{aligned}$$

Let us suppose that  $u = u_0 + \mu^{1/2}u_1 + \mu u_2 \dots$ . Substituting this, we get in the leading order

$$\partial_\tau u_0 = \partial_{xx} u_0,$$

which yields a uniform asymptotic state  $u_0 = \text{const.}$  We suppose  $u_0 = 1$ , like in the lattice model above.

In the next order, we get

$$\partial_\tau u_1 = \partial_x (\xi(x, \tau)) + \partial_{xx} u_1$$

which is the conserved version of the Edwards-Wilkinson (EW) equation.

Smith et al. [33] considered this EW equation and, in particular, demonstrated that the variance diverges (UV catastrophe). They did not perform a cutoff at the lattice size, but from their Eq. (8) it follows that  $\text{var}(u_1) \approx \ell^{-1}$  where  $\ell$  is the lattice spacing. The total variance is  $\text{var}(u) \approx \mu \ell^{-1}$ , in agreement with the result for the lattice model. Furthermore, from Gaussianity of  $\xi(x, t)$  it follows that the distribution of  $u_1$  is Gaussian. We show that the field  $u$  in the lattice TT model is indeed Gaussian in the limit  $\epsilon \rightarrow 1$  in Appendix B. Thus, we conclude that the limit  $\epsilon \rightarrow 1$  corresponds to the conserved version of the Edwards-Wilkinson stochastic differential equation.

### C. Field distribution

As mentioned above, we can solve Eq. (22) for the field distribution only in a special case  $\epsilon = 1/2$ . Numerical simulations have shown that for  $\epsilon < 1/2$ , the distribution has a power-law singularity at  $u \rightarrow 0$ , and cumulative distribution can be well approximated by a stretched exponential with a Gaussian cutoff:

$$P(> u) = \exp[-A(uL)^\alpha - B(uL)^2]. \quad (24)$$

We illustrate this in Fig. 11, where we show in rescaled coordinates the distributions for  $\epsilon = 0.1$  and  $\epsilon = 0.01$ .

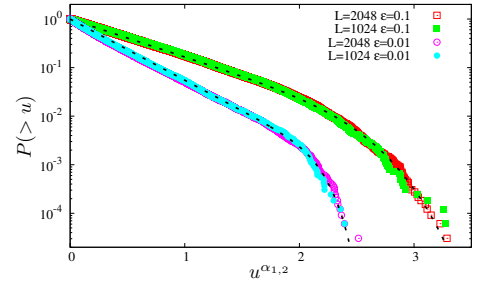


FIG. 11. Cumulative field distributions for  $\epsilon = 0.1$  and  $\epsilon = 0.01$ , and different  $L$ . Markers are the simulation data, dotted lines are fits with expression (24). For the exponents  $\alpha_{1,2}$  the theoretical expression (25) is used.

Although we cannot derive expression (24), we can estimate the exponent  $\alpha$  assuming the validity of (24). Let us suppose that the cumulative distribution  $P(>$

$u) = \int_u^\infty w(y) dy$  has the form of a stretched exponential  $P(> u) = \exp[-au^\alpha]$  for small  $u$  and  $\alpha < 1$ . Then, the density has a power law singularity at small  $u$  of the form

$$w(u) = a\alpha u^{\alpha-1} \exp[-au^\alpha] \approx Au^{\alpha-1}.$$

Let us look which value of  $\alpha$  is consistent with the Perron-Frobenius equation (22). Substituting, we get

$$\begin{aligned} Au^{\alpha-1} &\approx \\ \frac{1}{2} \frac{1}{\epsilon} A \frac{u^{\alpha-1}}{\epsilon^{\alpha-1}} + \frac{1}{2} \int_0^{u/(1-\epsilon)} A^2 (u - (1-\epsilon)v)^{\alpha-1} v^{\alpha-1} dv &= \\ \frac{Au^{\alpha-1}}{2\epsilon^\alpha} + \frac{A^2}{2(1-\epsilon)^\alpha} u^{2\alpha-1} \int_0^1 (1-z)^{\alpha-1} z^{\alpha-1} dz. \end{aligned}$$

Neglecting the last term, we obtain the consistency condition  $2\epsilon^\alpha = 1$  which means

$$\alpha = -\frac{\log 2}{\log \epsilon}. \quad (25)$$

This equation is in excellent agreement with the numerics as shown in Fig. (12).

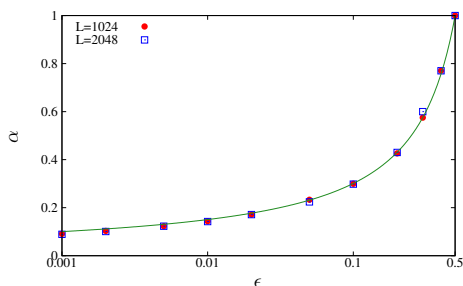


FIG. 12. Numerical values of the exponent  $\alpha$  of the stretched exponential part of the cumulative distribution (24) as a function of  $\epsilon$  (markers) together with the analytic estimate, Eq. (25).

#### D. Time correlations

In this section, we discuss the one-site temporal correlation function of the field (remember that we set  $\langle u \rangle = 1$ )

$$C(\Delta t) = \langle (u_n(t) - 1)(u_n(t + \Delta t) - 1) \rangle.$$

The calculated time-correlation function is shown in panel (a) of Fig 13. It appears that the correlations decay as a power law  $(\Delta t)^{-1/2}$ . In contrast, for  $L = 2$  the decay is exponential (see Appendix A and the panel (b) of Fig 13). Thus, one can expect a crossover at small  $L$ , we show in Fig 13(b) how correlations for a fixed  $\epsilon = 0.6$  depend on  $L$ . Here scaled coordinates are used; one can see that starting from  $L = 4$ , the scaling law  $C(\Delta t) \approx L^{-1} b (\Delta t L^2)^{-1/2} \exp[-a \Delta t L^2]$  works well (fitted values for  $a, b$  are in the caption).

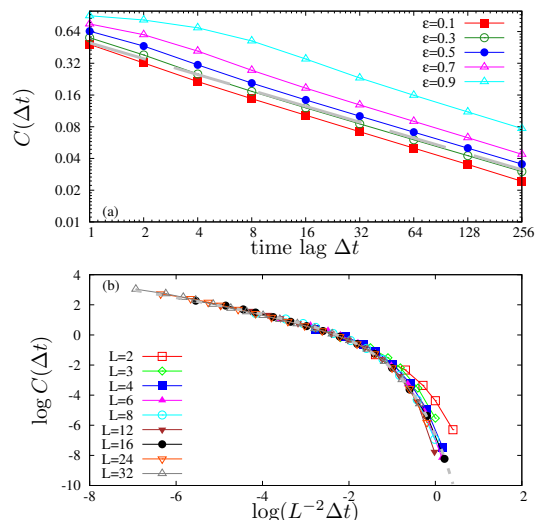


FIG. 13. Panel (a): Time-correlations functions for a lattice of length  $L = 1024$  and different  $\epsilon$ . The dashed grey line on this panel has a slope of  $-1/2$ . Panel (b): Time-correlations in scaling coordinates for different  $L$  and  $\epsilon = 0.6$ . The dashed gray line is a fit  $\log y = -0.511 - 0.5 \log x - 6.122 \exp(x)$ .

## VII. WEAK MICRODIFFUSION $\epsilon < L^{-1}$

### A. Hierarchical structure of peaks

We start our treatment of the case of very small microdiffusion with a visualization in Fig. 14 (a) of a snapshot of a field  $\{u_k\}$  in a statistically stationary regime (i.e., at times larger than characteristic transient time  $L^2$ ), at small values of microdiffusion parameter  $\epsilon$ . At  $\epsilon = 0$ , the field is just one peak (the maximal cluster) at which the whole initial “mass” is concentrated, at a random spatial position. For better comparison of fields for different sizes of the lattice  $L$ , we use below in this section the normalization  $\sum_k u_k = 1$ ; thus, the single peak for  $\epsilon = 0$  has mass one. Together with this maximal cluster, one observes in Fig. 14(a) peaks at different levels with a strong separation (several orders) between them.

To qualitatively understand this hierarchical structure of the field (which we will quantitatively characterize below), let us start with a single peak at  $\epsilon = 0$  and switch to a finite but small value of  $\epsilon$ . Then, the randomly moving main peak will leave behind secondary peaks of mass  $\approx \epsilon$ . These peaks will also move, leaving the next generation of peaks of mass  $\approx \epsilon^2$ ; they can also merge and be absorbed by the main peak (the size of which remains close to one – this is where the condition  $\epsilon L < 1$  plays its role). Thus, one can expect peaks at levels  $\sim \epsilon, \sim \epsilon^2, \sim \epsilon^3, \dots$ . However, this hierarchy is not very distinct, although recognizable, in the single profile at fixed  $\epsilon$ ; see the set of red circles or of blue squares in Fig. 14(a). To separate different levels in a more apparent way, we perform a simultaneous run of the TT model at two different values of parameter  $\epsilon$ :  $\epsilon_1$  and  $\epsilon_2$ . This means that the same

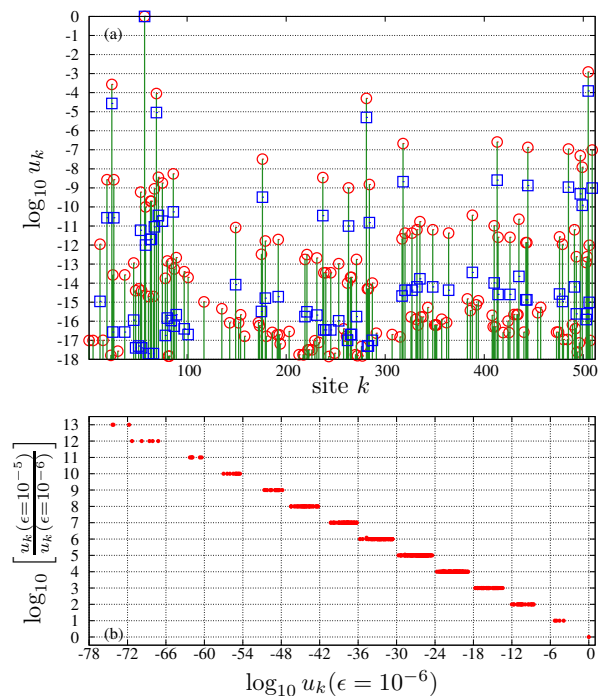


FIG. 14. Panel (a): Snapshots of the fields with  $\epsilon = 10^{-5}$  (red circles) and  $\epsilon = 10^{-6}$  (blue squares) for  $L = 512$ . Green lines show the positions of the main peaks (i.e., those with markers; there are many other peaks with masses smaller than  $10^{-18}$ , cf. bottom panel). Panel (b): The logarithmic difference in the levels of the peaks (i.e., the distance between red circles and blue squares of panel (a) at each peak) vs. the level of the blue squares.

random choices for advection steps (11) are chosen in two runs. As a result, the peaks in the two runs coincide in position but differ in their height by factor  $(\epsilon_1/\epsilon_2)^m$  with integer  $m$ . For an illustration in Fig. 14(a) we have chosen  $L = 512$ ,  $\epsilon_1 = 10^{-5}$  (red circles) and  $\epsilon_2 = 10^{-6}$  (blue squares). The grid in the  $y$ -axis corresponds to the ratio  $\epsilon_1/\epsilon_2 = 10$ . One can see that the main peaks in the two runs coincide. There are four peaks at the next level, with separation between them by factor  $\epsilon_1/\epsilon_2 = 10$ . The number of peaks at the next level is larger; there, the separation is  $(\epsilon_1/\epsilon_2)^2 = 100$ , etc. To make the correspondence of the separation and the level apparent, we plot in Fig. 14(b) all the  $L = 512$  values of  $\{u_k\}$  from the snapshot Fig. 14(a) in the coordinates “mass vs separation” (both axes logarithmic). One can see that the separations are very well “discretized” at integers of  $\log_{10}(\epsilon_1/\epsilon_2)$  ( $y$ -axis), while the levels in the field values are spread much wider ( $x$ -axis), and these widths for deep levels are of the same order as  $-\log_{10} \epsilon_2 = 6$ .

To illustrate that this hierarchical structure appears for small enough  $\epsilon$  only, we show in Fig. 15 the same plots as Fig. 14(b) for  $L = 1024$  and different values of  $\epsilon_1 = 10^{-m}$  and  $\epsilon_2 = 10\epsilon_1$ . One can see that the separation is apparent for  $m = 10, 9$  but becomes less distinct for  $m = 4$  and is practically not seen for large  $\epsilon$

( $m = 3$ ).

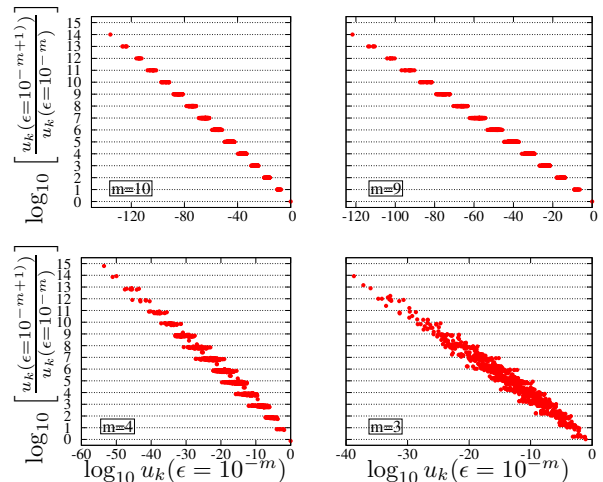


FIG. 15. The same plots as in Fig 14(b), but for different values of  $\epsilon = 10^{-m}$ . One can see that for large  $\epsilon$ , the order structure becomes blurry and eventually, no clear separation is seen for large  $\epsilon$ .

## B. Order kinetic model

In this Section, we present an effective model (termed “order kinetic model” (OKM)) to describe the structure observed in the simulation for small  $\epsilon$ , Figs. 14-15. Motivated by the observed hierarchical structure, we attribute to each site  $k$  an integer-valued order  $\mu_k$  and assume that the field  $u_k$  is represented as

$$u_k \approx \rho \epsilon^{\mu_k}. \quad (26)$$

Here  $\mu_k \geq 0$  is an integer called “order” of the field at site  $k$ . Parameter  $\rho \approx 1$  is a normalization factor (it roughly corresponds to the mass of the (unique) site having zero order in the asymptotic steady state). In the following, we will refer to the sites having the same value of  $\mu$  as the peaks of order  $\mu$  and denote by  $n(\mu)$  their number and by  $p(\mu) = n(\mu)/L$  their fraction (i.e., the probability to observe specific order). The expression (26) corresponds to an approximation in which the horizontal steps in Fig. 14(b) have zero width and zero height.

Let us now rewrite the update rule (11) in terms of the orders  $\mu_k$ , by considering two neighboring sites  $(i, j)$  corresponding respectively to orders  $(\mu_i, \mu_j)$ , with the direction of advection  $i \rightarrow j$ . Since the mass  $(1 - \epsilon)u_i$  is transferred to site  $j$  and the mass  $\epsilon u_i$  is left to site  $i$ , we write the following update rule for the orders:

$$\begin{aligned} \mu_i &\rightarrow \mu_i + 1, \\ \mu_j &\rightarrow \text{MIN}\{\mu_i, \mu_j\}. \end{aligned} \quad (27)$$

The approximation here follows from our perfect discretization of the levels: we neglect changes in the field,

if the addition is smaller than the existing field by factor  $\epsilon^m$ ,  $m \geq 0$ .

Special care should be taken about the sites with minimal possible order  $\mu_{min} = 0$ . As it follows from (27), the number of such sites can only decrease, and eventually, there is only one such site in the lattice. With one site having zero order, this situation is an absorbing state in model (27).

Before proceeding, we notice that the OKM (27) is, in fact, a skew (unidirectionally coupled) system: Higher-order peaks do not influence the zero-order peak; the first-order peaks interact only with each other (can coalesce) and with the zero-order peak (can be “emitted” or “absorbed” by it), etc. We will use this property in section VIID below.

### C. Mean field approach

In the framework of the OKM, one can apply the same mean-field approach as in Section VIA to write an equation for the evolution of the probabilities  $p(\mu)$ . The basic assumption is the independence of neighboring values of  $\mu_{i,j}$  in (27). Thus, the minimum MIN in (27) should be calculated as a minimum value of two independent random variables having the same distribution  $p(\mu)$ :

$$\text{prob}(\text{MIN}(\mu_i, \mu_j) > \mu) = \text{prob}(\mu_i > \mu) \cdot \text{prob}(\mu_j > \mu) = (1 - \text{prob}(\mu_i \leq \mu)) \cdot (1 - \text{prob}(\mu_j \leq \mu)).$$

This leads to the following expression for this distribution, valid for  $\mu \geq 1$  (this expression is analogous to (22)):

$$p(\mu) = \frac{1}{2}p(\mu-1) + \frac{1}{2} \left[ \left(1 - \sum_{\nu=0}^{\mu-1} p(\nu)\right)^2 - \left(1 - \sum_{\nu=0}^{\mu} p(\nu)\right)^2 \right]. \quad (28)$$

The first term corresponds to the case where the site is a “source” (this happens with probability 1/2); the second term corresponds to the case (also with probability 1/2) when the site is a “destination”. One can see from (28), that  $p(\mu)$  depends only on values  $p(\nu)$  with  $\nu < \mu$ . In terms of  $p(\mu)$ , expression (28) is a quadratic equation. Its solution begets a recursion relation

$$p(\mu) = \sqrt{s^2(\mu-1) + p(\mu-1)} - s(\mu-1), \quad (29)$$

$$s(\mu) = \sum_{\nu=0}^{\mu} p(\nu),$$

which has to be iterated started from  $p(0) = 1/L$ . We compare this solution with numerically obtained distribution in Figure 16. One can see that correspondence is not good, what indicates that in the TT model (11) the correlations between the neighboring sites are large and cannot be neglected. On the other hand, for the global coupled version of the TT model (12), where correlations are expected to be very small in the thermodynamic limit, the correspondence is very good.

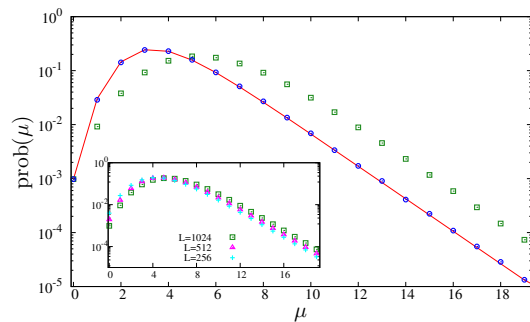


FIG. 16. Comparison of a theoretically obtained distribution of peaks  $p(\mu)$  (Eq. (29), red curve) with numerics for the TT model (green squares) and for the global coupled TT model (12), blue circles. All these data are for  $L = 1024$ . In the inset, we also show data for the TT model with  $L = 512$  and  $L = 256$ .

### D. Dynamics of lowest-order peaks

As demonstrated above, for the OKM, the mean-field approximation is not very successful because of correlations in the peak positions. Such a correlation is not very surprising because the first-order peaks are “daughters” of the zero-order peak and thus are located close to it; the same holds for other orders (“The apple never falls far from the tree”). To get insight, we visualize the dynamics of the peaks of orders  $\mu = 0, 1, 2$ . In Fig. 17, we compare the trajectories of the main (zeroth order) peak (blue) with the ones of peaks of order one (red) and two (green). One can clearly see that the first-order peaks are mainly in the vicinity of the zero-order peak (from which they are created), but some leave this vicinity, diffuse and merge. A similar creation-merging is observed at the bottom panel, where peaks of order one and two are depicted.

Let us now describe the relative motion of the main peak and the 1st order peaks. To this aim, let us focus on Figure 17 (middle panel), which shows the main peak (order 0) and the peaks of order 1. Let us redraw this figure by plotting the differences in the positions of the peaks of order one and the position of order zero; see Fig. 18 (in fact, here, another random realization is taken).

To describe Fig. 18, we can formulate a reduced version of the OKM (27), which takes into account only peaks of the 1st order (we denote their masses as  $w_k$ ) and the main one (zero-order peak). Moreover, it is instructive to go beyond the OKF and distinguish masses of the 1st-order peaks (although later, we will ignore them). Because the motions of the main peak and of other sites are independent, we place the main peak at zero and fix it. The dynamics of all other sites follows the KR model (TT model with  $\epsilon = 0$ ). Namely, at time  $t$ , a pair of points  $k, l$  is chosen randomly, with  $l = k \pm 1$ . If  $k = 0$ , then we set  $w_l(t+1) = w_l(t) + 1$ . If  $k \neq 0$  and  $l \neq 0$ , then the dynamics is as follows

$$w_k(t+1) = 0, \quad w_l(t+1) = w_l(t) + w_k(t).$$

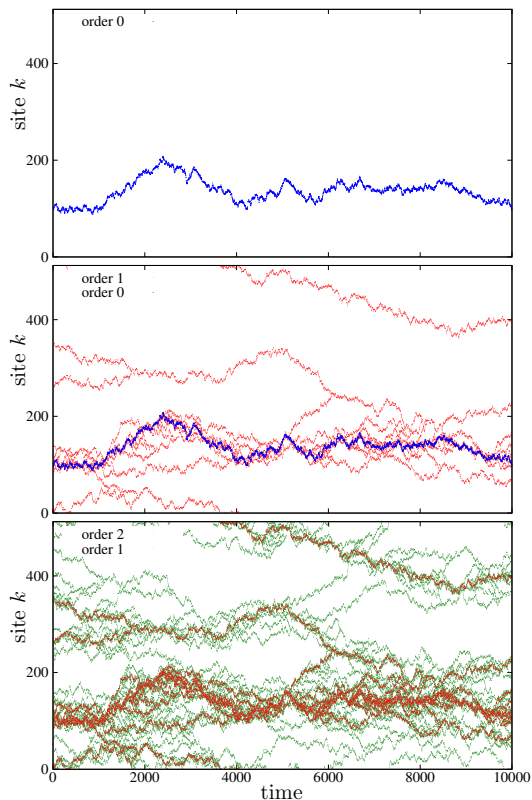


FIG. 17. Trajectories of peaks of order 0 (blue, upper panel), of order 0 (blue) and 1 (red) (middle panel), and of order 1 (red) and 2 (green) (bottom panel) (simulations of the TT model (11) for  $L = 512$ ,  $\epsilon = 10^{-6}$ ). Simulations were started from random initial conditions but an initial transient of duration  $L^2$  was dismissed.

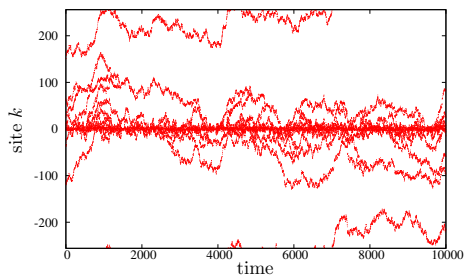


FIG. 18. Trajectories of the distances of the peaks of levels one from the main peak for  $L = 512$  (thus, the position of the main peak is at zero) in the TT model (11).

If  $k \neq 0$  and  $l = 0$ , then  $w_k(t+1) = 0$ . This dynamics in words: The mass of the main peak (located at the origin) is not varied. Instead, this peak randomly emits “daughters” of mass one. These first-order particles diffuse and coalesce. They disappear when the main peak absorbs them.

This model yields positions of the 1st order peaks that crowd around the main peak but can also leave its vicinity, making excursions to the “bulk” of the lattice. Note also that the model is not space-shift invariant because

we fix the main peak at the origin.

To characterize the crowding, it is important to distinguish two types of densities. One is  $\rho(k) = \langle w(\pm k, t) \rangle$  (here because of symmetry around zero, sites  $\pm k$  are considered equivalent). This is an average mass; peaks with higher mass (after one or several coalescence events) contribute more to this density.

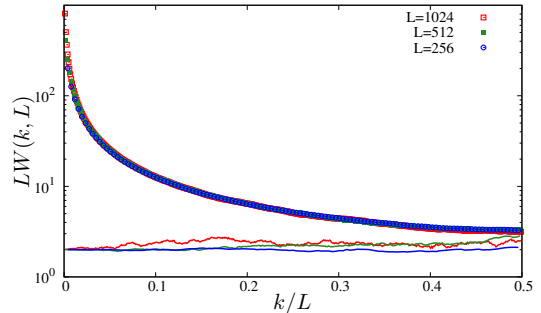


FIG. 19. Occupation densities  $W(k, L)$  (markers) of the 1st order peaks along the lattice for different  $L$ , in the scaled coordinates  $L \cdot W$  vs  $k/L$ . On this panel, the solid curves (the colors correspond to those of the markers) are non-normalized mass densities  $\rho$  vs  $k/L$ .

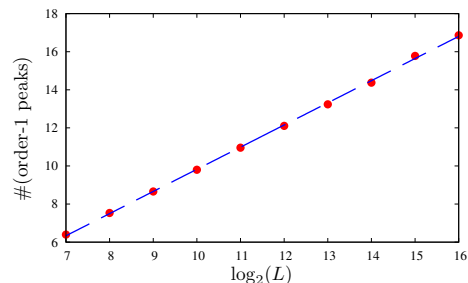


FIG. 20. Mean number of order-1 peaks as a function of lattice size  $L$  (markers). The dashed line is a linear fit.

Another density is  $W(k, t) = \langle 1 - \delta(w(\pm k, t)) \rangle$  where  $\delta(w) = 1$  if  $w > 0$  and  $\delta(w) = 0$  if  $w = 0$ . This density counts occupied sites, irrespective of the value of the mass  $w$  at these sites.

Because the motion of the peaks between interactions with the main peak at the origin is a pure diffusion, one expects that the stationary mass density  $\rho(k)$  is uniform. On the other hand, the occupation density  $W(k)$  decays due to collisions with other 1st order peaks, thus one expects that in the stationary state, it is maximal close to the origin and decays toward the bulk of the lattice.

We elaborate on statistical theory for the occupation density  $W(k, t)$  in Appendix C. This theory predicts that the stationary density scales with the lattice size  $L$  as  $W(k) = L^{-1} \hat{W}(k/L)$ . This relation is tested in Fig 19. We also confirm that  $\rho(k)$  is uniform in this figure.

Another prediction is that the average number of the 1st-order peaks growth with the lattice size as  $\sim \log L$ ; this relation is checked in Fig. 20. For higher-order

peaks, the dependence on  $\log L$  is nonlinear (not shown).

### VIII. DISCUSSION AND CONCLUSIONS

We start by summarizing our main findings. We have studied the statistical properties of KR and TT lattice models. The only two parameters are the redistribution constant  $\epsilon$  and the lattice size  $L$ . There are two main regimes:  $\epsilon \lesssim L^{-1}$ , where microdiffusion is small, and  $\epsilon \gtrsim L^{-1}$ , where microdiffusion is large. For small microdiffusion, one observes a concentration of almost all mass on a single randomly moving site (this concentration is perfect in the KR case,  $\epsilon = 0$ ). The masses on other sites are small, and for very small  $\epsilon$ , the dynamics builds a hierarchical structure, described in detail in Section VII. For large microdiffusion, a statistically uniform in space random regime establishes, described in section VI. In the limit  $\epsilon \rightarrow 1$  this regime corresponds to the Edward-Wilkinson equation with conserved noise.

It is instructive to compare the properties of the KR and TT models to other cases from the literature where mass-conserved models on a one-dimensional lattice (some with condensation/coagulation) have been studied.

The foremost feature of all models studied in this paper and summarized in Fig. 2 is that the average density  $\rho$  is a scalable parameter; therefore, it can't act like a control parameter and no (equilibrium or out-of-equilibrium) phase transition can appear when tuning  $\rho$ . Not even at  $\rho = 0$  because the model is not defined in the absence of mass. This property is, of course, shared with the random advection-diffusion equation (6).

Nonetheless, it is interesting to analyze our models in terms of *condensation*, a process occurring when a finite fraction of the total mass/energy is localized on a finite number of sites; in our language this corresponds to the formation of a maximal cluster.

Adopting a strict point of view according to which a phase transition only occurs in the thermodynamic limit, the only model displaying condensation is KR, whose steady state corresponds to a single site hosting the whole mass. However, considering the mass distribution at finite size  $L$ , the TT model has remarkable features because the degree of condensation depends on the product of the intensive parameter  $\epsilon$  and the extensive parameter  $L$ : we have a sort of finite-size condensation for lattices with  $L \lesssim 1/\epsilon$ . On this scale (which diverges for  $\epsilon \rightarrow 0$ ), almost all mass is concentrated on a single site (a zero-order peak), as described in Section VII.

We add that such finite-size condensation is attained via a dynamic coarsening, in which the condensed fraction increases with time. This phenomenon is visible in the roughness increase with time, as described in Sec. V.

When comparing different models, the deterministic *versus* random rule to redistribute the mass is an important feature. In the TT model, the parameter  $\epsilon$  is fixed, but it could be chosen randomly in the unitary

interval, obtaining effectively the “random TT model”, which has been studied (although not with this name) by Rajesh and Majumdar in Ref. [21] (it corresponds to their symmetric model in the limit of continuous-time dynamics). Thus we denoted it RM in Section III A. The phenomenology of such a model is fairly different from ours, which is strongly dependent on  $\epsilon L$ , a parameter that is nonsense if  $\epsilon$  is random.

It is also instructive to compare with the Kipnis-Marchoro-Presutti (KMP) model [20], where a pair of sites  $(k, k \pm 1)$  is chosen randomly and the masses are redistributed according to

$$u'_k = \xi(u_k + u_{k\pm 1}), \quad u'_{k\pm 1} = (1 - \xi)(u_k + u_{k\pm 1}), \quad (30)$$

$\xi$  being a random number uniformly distributed in  $(0, 1]$ . In Ref. [20], it has been proven that a stationary distribution in the KMP model is an equilibrium Gibbs distribution. This is not surprising because the update rule (30) satisfies the detailed balance condition. This is in contradistinction to the TT model (even in its random version), where the detailed balance is not valid. KMP is the prototypical example of diffusion, therefore, of a smoothing process. It is, therefore, interesting to consider its deterministic counterpart (det-KMP in Section III A), where  $\xi$  is fixed, and we denote  $\xi = \epsilon$ . In the limit  $\epsilon = 0$ , it is the same as the KR model; we might therefore think that for small  $\epsilon$  it is similar to the TT model. Before considering this possibility, we should note that the det-KMP model is invariant under the transformation  $\epsilon \rightarrow 1 - \epsilon$ , which sets  $1/2$  as the maximal value of  $\epsilon$ . For this reason, when reproducing Fig. 8 for the det-KMP model, we have replaced  $\epsilon/(1 - \epsilon)$  (see the label of the horizontal axis) with  $\epsilon/(0.5 - \epsilon)$ . The result is plotted in Fig. 21, showing a strong resemblance between the two *deterministic* models. We emphasize “deterministic” to stress that the TT model is far more similar to det-KMP than to the random version of itself (RM).

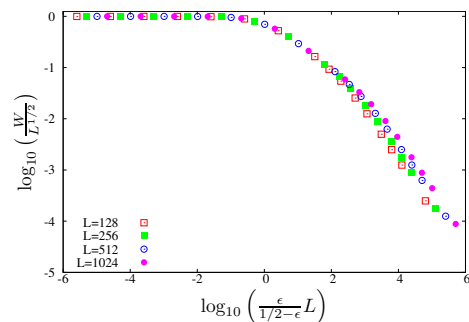


FIG. 21. Saturated width of the interface in the det-KMP model in scaled coordinates, for different  $\epsilon$  and different lattice sizes. This plot is very similar to Fig. 8, suggesting that the det-KMP model probably has the same statistical properties as the TT model.

It is worth stressing a further difference between the finite-size localization found in TT and det-KMP and the standard condensation process found in models where

the density  $\rho$  (density of mass or other conserved quantity) plays the role of the control parameter. There is a plethora of such models, and it is not the case to review them, here we limit to say that condensation exists if  $\rho$  is larger than some critical value  $\rho_c$  (we will give a specific example later). Let us now try a parallel between the standard condensed phase appearing for  $\rho > \rho_c$ , and the finite-size localized phase found in TT and det-KMP models when  $\epsilon < \epsilon_c = 1/L$ . In both cases, we have a condensate in equilibrium with a background and, for large  $L$ , the condensate is composed of a single site hosting a macroscopically large peak. Let us now imagine removing the condensate: in the TT model, the density is scalable, and a new condensate will spontaneously appear. Instead, in the standard condensation models, this will not occur because removing the condensate will also reduce the density to its critical value,  $\rho \rightarrow \rho_c$ . We stress that this is not just a trivial reformulation due to the different physical nature of the two control parameters  $\rho$  and  $\epsilon$  (a “density” *versus* “not a density”), but a consequence of a different dynamical behavior in the condensed phase. In standard condensation models, the condensate and the background belong to two different equilibrium phases, and the removal of the condensate does not affect the background. In the TT model, there is really no such distinction, as clarified by the order kinetic model above.

To obtain a standard condensation transition where the density does play the role of a control parameter, it is necessary to introduce a physical scale of the mass. For this reason, we conclude this discussion by mentioning a chipping model (CM) [34, 35] where the mass  $u_i$  is a non-negative *integer* and which seems to have some features similar to the TT model. Here mass is transported symmetrically to one of the neighboring sites with two distinct and parallel processes: (i) The whole mass (i.e., all particles) is transported from site  $i$  to site  $i \pm 1$ . This occurs with rate 1. (ii) One single particle (if existing) is transported from site  $i$  to site  $i \pm 1$ . This occurs with rate  $w$ . This model displays condensation for  $\rho > \rho_c = \sqrt{1+w} - 1$ .

If  $w = 0$ , then  $\rho_c = 0$ , and this model is equivalent to the KR model, displaying the formation of a single cluster containing all the mass. If  $\rho \gg 1$ , the discrete nature of the mass is not relevant, and for diverging  $w$  CM is similar to the TT model for  $(1 - \epsilon) \ll 1$ , which explains why it does not display condensation. The CM model is another simple example of a lattice with a clear separation of micro- and macro-diffusion: for  $w = 0$  there is only macrodiffusion, for  $w = \infty$  there is only microdiffusion. For finite values of  $w$ , their relative importance depends on the mass density.

In this manuscript, we have proposed a unifying picture to gather several models of local mass transport under the same umbrella, see Fig. 2. It seems to us that different models, also including models not covered by such an umbrella, e.g., the just-mentioned CM model, might be discussed in terms of micro/macro diffusion, macrodiffusion being a key element in obtaining a condensation-

like phenomenon and microdiffusion being the obstacle to it. In particular, we have discussed in detail a deterministic process where a single parameter  $\epsilon$  allows to switch between the two cases.

Since we have shown that the deterministic or random nature of the parameters  $a, b$  entering in the definition of the generic two-site model, see Sec. III A, is of crucial importance, it might be of interest to distinguish between these two classes and determine the ensemble of models of each class displaying condensation.

## ACKNOWLEDGMENTS

We thank P. Grassberger for the valuable discussions. AP acknowledges hospitality of ISC-CNR in Florence.

### Appendix A: The TT model as an IFS

In this appendix, we demonstrate fractal properties of the invariant distribution in the TT (11) model for small lattice lengths, adopting the Iterated Function Systems (IFS) concept.

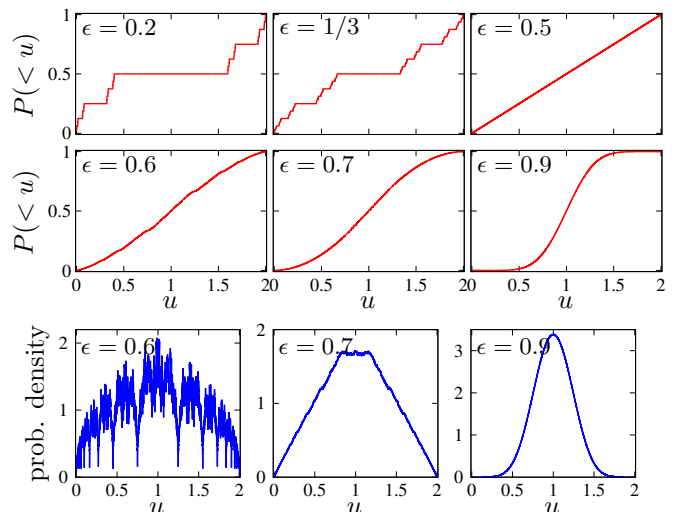


FIG. 22. The cumulative distribution  $P(<u)$  in the IFS system (A1) for different  $\epsilon$  (upper two panels). This distribution is a classical fractal for  $\epsilon < 1/2$ . The distribution is continuous for  $\epsilon > 1/2$  but becomes smooth only for large  $\epsilon$ . Bottom panel: densities for cases  $\epsilon > 1/2$ .

#### 1. Case $L = 2$ : Bernoulli convolution

Let us consider the minimal case  $L = 2$  and  $u_1 + u_2 = 2$ . Because of the conservation law, we have just one nontrivial variable  $u$ , since another variable is expressed

as  $2 - u$ . In this case the transformation (21) reads

$$u(t+1) = \begin{cases} \epsilon u(t) & \text{Prob } 1/2, \\ \epsilon u(t) + 2(1 - \epsilon) & \text{Prob } 1/2. \end{cases} \quad (\text{A1})$$

This one-dimensional IFS is the so-called Bernoulli convolution [36–38]. Bernoulli convolution generates a classical fractal if  $\epsilon < 1/2$ , and a relatively smooth distribution without voids for  $\epsilon > 1/2$ , see [39, 40]. [For  $\epsilon = 1/2$ , the invariant distribution is uniform.] The expression for the dimension (there is only one dimension for  $\epsilon < 1/2$ , the set is a mono-fractal) is a trivial application of the scaling relation:  $d = -\frac{\log 2}{\log \epsilon}$  and is smaller than one for  $\epsilon < 1/2$ . In Fig. 22, fractal and smooth examples are presented [39, 40].

It is straightforward, using linearity of (A1), to calculate statistical properties of  $u(t)$  (cf. [41]). The average is  $\langle u \rangle = 1$ . For the autocorrelation function  $C(t) = \langle (u(t) - 1)(u(0) - 1) \rangle$  one easily obtains a recursion  $C(t+1) = \epsilon C(t)$ , from which the exponential decay of correlations follows  $C(t) = C(0)\epsilon^t$ .

## 2. Case $L = 3$

In this case, because of the conservation law  $u_1 + u_2 + u_3 = 3$ , the dynamics lies on a two-dimensional simplex. Several images of the distribution ( $10^4$  points are drawn) are shown in Fig. 23. Like in the case  $L = 2$ , the distribution is without voids for  $\epsilon \geq 0.5$  and a fractal measure with a hierarchy of voids for  $\epsilon < 0.5$ .

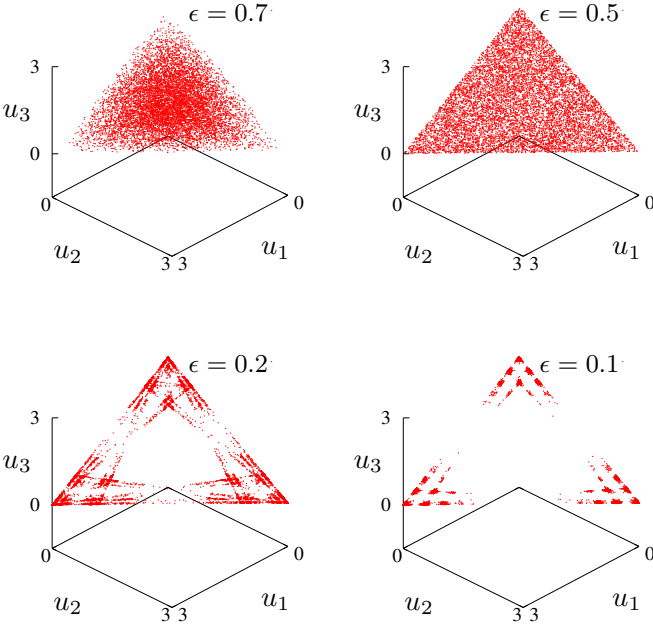


FIG. 23. Distributions of fields  $(u_1, u_2, u_3)$  for  $L = 3$  and several values of  $\epsilon$ .

## Appendix B: Gaussianity of the field distribution in the limit $\epsilon \rightarrow 1$

Here we rewrite the TT model using  $\mu = 1 - \epsilon \ll 1$ :

$$\bar{u} = \begin{cases} (1 - \mu)u & \text{prob } 1/2, \\ u + \mu u_{\pm} & \text{prob } 1/2. \end{cases}$$

Let us introduce the characteristic function  $C(k) = \langle e^{iku} \rangle$  and assume that  $u$  and  $u_{\pm}$  are statistically independent. Then the Perron-Frobenius equation for  $C$  reads

$$\bar{C}(k) = \frac{1}{2}C(k(1 - \mu)) + \frac{1}{2}C(k)C(k\mu).$$

In the stationary situation  $\bar{C} = C$  and we obtain

$$2 = C(\mu k) + \frac{C((1 - \mu)k)}{C(k)}. \quad (\text{B1})$$

Because the mean value of  $u$  is arbitrary, we set it to one. Then the characteristic function can be written in terms of cumulants  $\kappa_m$ ,  $m \geq 2$ :

$$C(k) = \exp \left[ ik + \sum_{m=2}^{\infty} \kappa_m \frac{k^m}{m!} \right].$$

For the ratio of characteristic functions, we get

$$\begin{aligned} \frac{C((1 - \mu)k)}{C(k)} &= \exp[-ik\mu + \kappa_2 \frac{k^2}{2}(-2\mu + \mu^2) + \\ &+ \kappa_3 \frac{k^3}{6}(-3\mu + 3\mu^2 - \mu^3) + \dots]. \end{aligned}$$

The equation for  $C$  (B1) then reads

$$\begin{aligned} 2 &= \exp[-ik\mu + \kappa_2 \frac{k^2}{2}(-2\mu + \mu^2) + \\ &+ \kappa_3 \frac{k^3}{6}(-3\mu + 3\mu^2 - \mu^3) + \dots] + \\ &+ \exp[ik\mu + \kappa_2 \mu^2 \frac{k^2}{2} + \kappa_3 \mu^3 \frac{k^3}{6} + \dots]. \end{aligned}$$

We now expand the r.h.s. keeping orders  $\mu^0, \mu^1, \mu^2$  only:

$$\begin{aligned} 2 &= 2 + \mu[-\kappa_2 k^2 - \kappa_3 \frac{k^3}{2} - \kappa_4 \frac{k^4}{6} - \dots] - \mu^2 k^2 + \\ &\mu^2 [\kappa_2 \frac{k^2}{2} + \kappa_3 \frac{k^3}{2} + \kappa_4 \frac{k^4}{4} + \dots] \end{aligned}$$

Comparing terms at  $k^2$ , in the leading order in  $\mu$ , we get  $\kappa_2 = \mu$ . Comparing terms at  $k^3, k^4, \dots$  we get  $\kappa_3 = \kappa_4 = \dots = 0$ . This proves that for  $\mu \rightarrow 0$  the field is Gaussian, with the variance  $\kappa_2 = \mu$ .

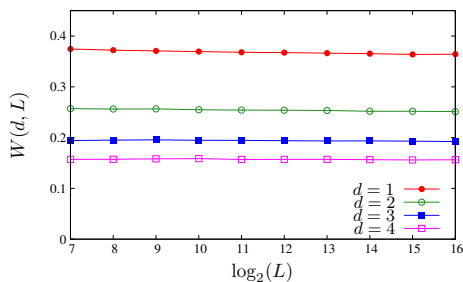


FIG. 24. Mean occupations of the sites  $W(k=d)$  close to the main peak (which is at  $k=0$ ), for different sizes of the lattice  $L$ . The closest neighbor site has occupation  $\approx 0.37$ .

### Appendix C: Statistical theory for the occupation density of first-order peaks

Here we derive, within the OKM, an equation for the evolution of the occupation density of first-order peaks (treated as particles)  $W(k, t)$ , in a lattice of length  $L$ . First, we replace  $k$  with a continuous coordinate  $0 \leq x \leq L$ . The basic dynamics is a diffusion of particles; thus, we start with the diffusion equation  $\partial_t W(x, t) = D \partial_{xx} W(x, t)$ .

Due to the coalescence of particles, the number of occupation sites decreases. Therefore one should add a damping term. To elaborate on it, consider a spatially homogeneous state with constant density  $W$ . Then the distance between the particles is  $X \approx W^{-1}$ . The time for two particles to coalesce is the diffusion time for the distance between the peaks, i.e.  $t_c \approx X^2/D$ . The rate of coalescence is therefore  $t_c^{-1} = DX^{-2} = DW^2$ . Thus from the equation  $\partial_t (\ln W) = -DW^2$  we get the damping term  $\partial_t W = -DW^3$ . We notice that the spatially homogeneous solution  $W(t) = \frac{W(0)}{\sqrt{1+2DW^2(0)(t-t_0)}}$  yields the asymptotic time dependence  $W \sim t^{-1/2}$ , which is confirmed by numerics.

However, in our case, the occupation density is inhomogeneous because particles are created at  $x=0$  (or, equivalently, at  $x=L$ ), where the main peak is placed. The sites near the main peak are predominantly occupied; therefore, we can assume a constant occupation  $W=c$  at this boundary. To check that the density at the boundary does not depend on  $L$ , we calculated this density numerically at sites adjacent to the main peak in the TT model; see results in Fig. 24. This figure shows that the occupation of the nearest neighbor to the peak is around 0.37, almost independent on  $L$ .

Summarizing, we have the following PDE and bound-

ary conditions for the occupation density  $W(x, t)$ :

$$\frac{\partial W(x, t)}{\partial t} = D \frac{\partial^2 W}{\partial x^2} - DW^3, \quad W(0, t) = W(L, t) = c.$$

The stationary solution  $W(x)$  of this equation obeys

$$\frac{d^2 W}{dx^2} - W^3 = 0, \quad W(0) = W(L) = c.$$

We can integrate once and obtain

$$\begin{aligned} \frac{1}{2} \left( \frac{dW}{dx} \right)^2 - \frac{1}{4} W^4 &= -\frac{w^4}{4}; \\ \frac{dW}{dx} &= \pm \frac{1}{\sqrt{2}} \sqrt{W^4 - w^4}, \end{aligned} \quad (\text{C1})$$

where we took as a constant  $w = W_{min} = W(L/2)$ . Integration of this equation on the interval  $0 \leq x \leq L/2$  yields

$$\frac{wL}{2\sqrt{2}} = \int_1^{c w^{-1}} \frac{dy}{\sqrt{y^4 - 1}} = \frac{1}{\sqrt{2}} F(\arccos \frac{w}{c}, \sqrt{2}/2),$$

where  $F(\phi, k)$  is the elliptic integral of the 1st kind. The constant  $w$  should be obtained self-consistently from this relation. If we assume  $w \ll 1$ , what is to be expected for large lattice sizes  $L$ , then  $F(0, k) = \pi/2$  and we get a relation

$$wL = \pi.$$

Substituting this in (C1), we can represent the stationary occupation density as  $W(x) = \frac{\pi}{L} Q(\frac{x}{L})$ , where  $Q(z)$  is a solution of ODE  $\frac{dQ}{dz} = -\pi 2^{-1/2} \sqrt{Q^4 - 1}$  with initial condition  $Q(0) = cL\pi^{-1}$ . This relation agrees with data in Fig. 19(b).

We can calculate the average number of particles in the lattice from the derived distribution. The total number of order-1 peaks is

$$\begin{aligned} K &= 2 \int_0^{L/2} W(x) dx = 2\sqrt{2} \int_w^c \frac{W dW}{\sqrt{W^4 - w^4}} = \\ &= \sqrt{2} \int_1^{c^2 w^{-2}} \frac{dy}{\sqrt{y^2 - 1}} = 2^{1/2} \ln(y + \sqrt{y^2 - 1}) \Big|_1^{c^2 w^{-2}} \\ &\approx 2^{3/2} \ln L, \end{aligned}$$

where in the last expression we assumed  $w \ll 1$  and neglected  $\ln c\pi$ . The numerical dependence of  $K$  on  $\ln L$  is presented in Fig. 20.

- 
- [1] Zellman Warhaft, “Passive scalars in turbulent flows,” *Annual Review of Fluid Mechanics* **32**, 203–240 (2000).  
 [2] Robert H. Kraichnan, “Anomalous scaling of a randomly advected passive scalar,” *Phys. Rev. Lett.* **72**, 1016–1019

(1994).

- [3] Tov Elperin, Nathan Kleeorin, and Igor Rogachevskii, “Dynamics of the passive scalar in compressible turbulent flow: Large-scale patterns and small-scale fluctuations,”

- Phys. Rev. E **52**, 2617–2634 (1995).
- [4] Angelo Vulpiani, Fabio Cecconi, and Massimo Cencini, *Chaos: from simple models to complex systems*, Vol. 17 (World Scientific, 2009).
  - [5] JM Deutsch, “Probability distributions for multicomponent systems with multiplicative noise,” *Physica A: Statistical Mechanics and its Applications* **208**, 445–461 (1994).
  - [6] Stefano Lepri, “Fluctuations in a diffusive medium with gain,” *Phys. Rev. Lett.* **110**, 230603 (2013).
  - [7] F. Leyvraz, “Scaling theory and exactly solved models in the kinetics of irreversible aggregation,” *Physics Reports* **383**, 95–212 (2003).
  - [8] A. S. Pikovsky, “Synchronization and stochastization of the ensemble of autogenerators by external noise,” *Radiophys. Quantum Electron.* **27**, 390–395 (1984).
  - [9] V. A. Antonov, “Modeling of processes of cyclic evolution type. synchronization by a random signal.” *Proceedings of Leningrad University, Astronomy (in Russian)*, 67–76 (1984).
  - [10] H. Crauel and F. Flandoli, “Attractors for random dynamical systems,” *Probab. Theory Relat. Fields* **100**, 365–393 (1994).
  - [11] Z. F. Mainen and T. J. Sejnowski, “Reliability of spike timing in neocortical neurons,” *Science* **268**, 1503 (1995).
  - [12] P. Khoury, M. A. Lieberman, and A. J. Lichtenberg, “Experimental measurement of the degree of chaotic synchronization using a distribution exponent,” *Phys. Rev. E* **57**, 5448–5466 (1998).
  - [13] A. Uchida, R. McAllister, and R. Roy, “Consistency of nonlinear system response to complex drive signals,” *Phys. Rev. Lett.* **93**, 244102 (2004).
  - [14] A. S. Pikovsky, “Statistics of trajectory separation in noisy dynamical systems,” *Phys. Lett. A* **165**, 33 (1992).
  - [15] J. C. Sommerer and E. Ott, “Particles floating on a moving fluid: a dynamically comprehensible physical fractal,” *Science* **259**, 335 (1993).
  - [16] K. Gawedzki and M. Vergassola, “Phase transition in the passive scalar advection,” *Physica D* **138**, 63–90 (2000).
  - [17] T. Bohr and A. S. Pikovsky, “Anomalous diffusion in the Kuramoto – Sivashinsky equation,” *Phys. Rev. Lett.* **70**, 2892–2895 (1993).
  - [18] K Kang and S Redner, “Fluctuation effects in Smoluchowski reaction kinetics,” *Physical Review A* **30**, 2833 (1984).
  - [19] Hideki Takayasu and Yh Taguchi, “Non-Gaussian distribution in random advection dynamics,” *Physical Review Letters* **70**, 782 (1993).
  - [20] C Kipnis, Carlo Marchioro, and E Presutti, “Heat flow in an exactly solvable model,” *Journal of Statistical Physics* **27**, 65–74 (1982).
  - [21] R Rajesh and Satya N Majumdar, “Conserved mass models and particle systems in one dimension,” *J. Stat. Phys.* **99**, 943–965 (2000).
  - [22] Supriya Krishnamurthy, R Rajesh, and Oleg Zaboronki, “Persistence properties of a system of coagulating and annihilating random walkers,” *Physical Review E* **68**, 046103 (2003).
  - [23] Our notation is different from the notation of the original paper [19] that employed the parameter  $j = 1 - \epsilon$ . Our choice is due to our interest towards the limit  $\epsilon \rightarrow 0$ .
  - [24] At first glance this statement is not obvious because the limit  $\epsilon \rightarrow 1$  might not commute with the thermodynamic limit  $L \rightarrow \infty$ . However we will provide a consistent description for any  $L$  and  $\epsilon$ .
  - [25] Misako Takayasu, Hideki Takayasu, and Yh Taguchi, “Non-Gaussian distribution in random transport dynamics,” *International Journal of Modern Physics B* **8**, 3887–3961 (1994).
  - [26] Hideki Takayasu, Takuo Kawakami, Y-h Taguchi, and Tomoo Katsuyama, “Fractal limit distributions in random transports,” *Fractals* **4**, 257–264 (1996).
  - [27] Michael F. Barnsley, *Fractals everywhere* (Academic press, 2014).
  - [28] The implementation of the latter property explains why we choose  $m/L$  rather than  $t/L^2$  as second argument of  $F_2(x, y)$ .
  - [29] Fereydoon Family and Tamas Vicsek, “Scaling of the active zone in the eden process on percolation networks and the ballistic deposition model,” *Journal of Physics A: Mathematical and General* **18**, L75 (1985).
  - [30] Tao Sun, Hong Guo, and Martin Grant, “Dynamics of driven interfaces with a conservation law,” *Physical Review A* **40**, 6763 (1989).
  - [31] Joachim Krug, “Origins of scale invariance in growth processes,” *Advances in Physics* **46**, 139–282 (1997).
  - [32] Fernando Caballero, Cesare Nardini, Frédéric van Wijland, and Michael E Cates, “Strong coupling in conserved surface roughening: a new universality class?” *Physical review letters* **121**, 020601 (2018).
  - [33] Naftali R. Smith, Baruch Meerson, and Pavel V. Sasorov, “Local average height distribution of fluctuating interfaces,” *Phys. Rev. E* **95**, 012134 (2017).
  - [34] Satya N. Majumdar, Supriya Krishnamurthy, and Mustansir Barma, “Nonequilibrium phase transitions in models of aggregation, adsorption, and dissociation,” *Phys. Rev. Lett.* **81**, 3691–3694 (1998).
  - [35] R Rajesh and Satya N Majumdar, “Exact phase diagram of a model with aggregation and chipping,” *Physical Review E* **63**, 036114 (2001).
  - [36] Yuval Peres, Wilhelm Schlag, and Boris Solomyak, “Sixty years of bernoulli convolutions,” in *Fractal geometry and stochastics II* (Springer, 2000) pp. 39–65.
  - [37] Simon J Fraser and Raymond Kapral, “Periodic dichotomous-noise-induced transitions and stochastic coherence,” *Physical Review A* **45**, 3412 (1992).
  - [38] Raymond Kapral and Simon J Fraser, “Dynamics of oscillators with periodic dichotomous noise,” *Journal of Statistical physics* **70**, 61–76 (1993).
  - [39] Yuval Peres, Károly Simon, and Boris Solomyak, “Absolute continuity for random iterated function systems with overlaps,” *Journal of the London Mathematical Society* **74**, 739–756 (2006).
  - [40] Julien Barral and De-Jun Feng, “On multifractal formalism for self-similar measures with overlaps,” *Mathematische Zeitschrift* **298**, 359–383 (2021).
  - [41] Arkady Pikovsky and Lev. S. Tsimring, “Statistical theory of asymmetric damage segregation in clonal cell populations,” *Mathematical Biosciences* **358**, 108980 (2023).